

# The Lennard-Jones Potential Revisited: Analytical Expressions for Vibrational Effects in Cubic and Hexagonal Close-Packed Lattices

Published as part of *The Journal of Physical Chemistry* virtual special issue "Alexander Boldyrev Festschrift".

Peter Schwerdtfeger,\* Antony Burrows, and Odile R. Smits



Cite This: *J. Phys. Chem. A* 2021, 125, 3037–3057



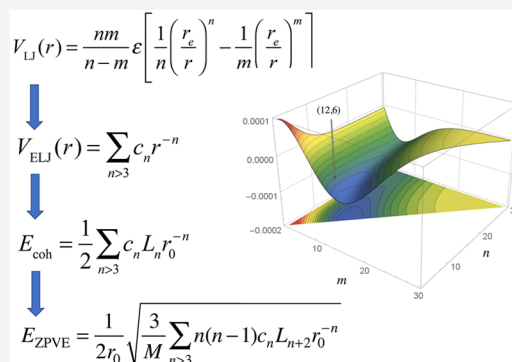
Read Online

ACCESS |

Metrics & More

Article Recommendations

**ABSTRACT:** Analytical formulas are derived for the zero-point vibrational energy and anharmonicity corrections of the cohesive energy and the mode Grüneisen parameter within the Einstein model for the cubic lattices (sc, bcc, and fcc) and for the hexagonal close-packed structure. This extends the work done by Lennard-Jones and Ingham in 1924, Corner in 1939, and Wallace in 1965. The formulas are based on the description of two-body energy contributions by an inverse power expansion (extended Lennard-Jones potential). These make use of three-dimensional lattice sums, which can be transformed to fast converging series and accurately determined by various expansion techniques. We apply these new lattice sum expressions to the rare gas solids and discuss associated critical points. The derived formulas give qualitative but nevertheless deep insight into vibrational effects in solids from the lightest (helium) to the heaviest rare gas element (oganesson), both presenting special cases because of strong quantum effects for the former and strong relativistic effects for the latter.



## INTRODUCTION

The  $(n, m)$  Lennard-Jones (LJ) potential<sup>1–5</sup> is, beside the Morse potential,<sup>6</sup> the most widely used interaction potential in the physical and biological sciences,<sup>7–11</sup>

$$V_{LJ}(r) = \frac{nm}{n-m} \epsilon \left[ \frac{1}{n} \left( \frac{r_e}{r} \right)^n - \frac{1}{m} \left( \frac{r_e}{r} \right)^m \right] \quad (1)$$

with an equilibrium distance  $r_e$  and binding energy  $\epsilon$  (taken as a positive value) between two interacting systems.

The story of how this interaction potential came to be commonly known today as the LJ potential started with Mie's 1903 discussion suggesting an equation of state containing a volume dependent term of the form  $(AV^{-1} - BV^{-\nu/3})$  with  $\nu > 3$ .<sup>12</sup> Following this, in 1912, Grüneisen<sup>13</sup> published the exact formula for what became the well-known  $(n, m)$  LJ potential, and in 1920, Kratzer also introduced a less general  $(2,1)$  potential which went unnoticed.<sup>14</sup> The Grüneisen  $(n, m)$  potential was modified by Born and Landé<sup>15</sup> in 1918 for ionic crystals, and the same year, Madelung introduced the lattice sum for ionic crystals today known as the Madelung constant.<sup>16</sup> It was not until 1924 after Lennard-Jones solved the equation of state analytically to derive the parameters based on experimental results, that the LJ  $(n, m)$  potential gained notoriety.<sup>1</sup> However, the physical relevance of the long-range dispersive term came much later in 1930 by London.<sup>17</sup> What is curious about the chronology is that Simon and Simpson used the Grüneisen

potential in 1924 giving it a proper citation, and Lennard-Jones in his second paper also cited Simon and Simpson's paper in 1924, but Grüneisen's paper was ignored.

To allow for a more accurate description of the interacting potential, the LJ potential has been generalized into an inverse power series of the form<sup>18,19</sup>

$$V_{ELJ}(r) = \sum_{n=1}^{n_{\max}} c_n r^{-s_n} \quad (2)$$

with  $c_n \in \mathbb{R}$  and  $s_n \in \mathbb{R}_+$  ( $s_1 = 6$  and  $s_2 = 12$  for the  $(12, 6)$  LJ potential). A boundary condition such that the minimum is positioned at a distance  $r_e$  with a potential depth of  $\epsilon$  such that  $\sum_{n=1}^{n_{\max}} c_n r_e^{-s_n} = -\epsilon$  with  $\epsilon > 0$ . The coefficients  $c_n$  can be obtained from either experimental data or accurate quantum-theoretical calculations.<sup>19,20</sup> The advantage of the inverse power series compared to more complicated expressions like the Morse potential,<sup>6</sup> or accurate potential forms separating the long-range from the short-range region,<sup>21–23</sup> is that one can express

Received: January 1, 2021

Revised: February 28, 2021

Published: March 31, 2021



analytically the volume dependent two-body (static) cohesive energy of certain lattices in terms of infinite lattice sums,

$$\begin{aligned} E_{\text{ELJ}}(V) &= \lim_{N \rightarrow \infty} \frac{1}{N} \sum_{i < j}^N V_{\text{ELJ}}(r_{ij}) = \frac{1}{2} \sum_{i=1}^{\infty} V_{\text{ELJ}}(r_{0i}) \\ &= \frac{1}{2} \sum_{n=1}^{n_{\max}} c_n L_{s_n} r_0^{-s_n} = \frac{1}{2} \sum_{n=1}^{n_{\max}} f_L^{s_n/3} c_n L_{s_n} V^{-s_n/3}. \end{aligned} \quad (3)$$

Here,  $n > m$  guarantees the existence of a minimum and  $s_n > 3$  to guarantee convergence for the 3D bulk system.<sup>19</sup> In eq 3,  $r_0$  is the nearest neighbor distance of the lattice  $r_0 = \min\{r_{0i}\}$ , with  $r_{0i}$  being the distance from one selected atom in the lattice to all other atoms  $i$ , and  $f_L$  is a lattice-specific parameter converting  $r_0$  into the volume  $V = f_L r_0^3$ , i.e.,  $f_{\text{sc}} = 1$ ,  $f_{\text{bcc}} = 4/(3\sqrt{3})$ ,  $f_{\text{fcc}} = f_{\text{hcp}} = 1/\sqrt{2}$ . We use the fact that for a cubic lattice the summation over all atoms  $i$  and  $j$  with distance  $r_{ij}$  simplifies to summing over all interactions from one selected atom placed at the origin to all other atoms  $i$  in the solid because of translational symmetry. Once basic lattice vectors are introduced to express the distances  $r_{0i}$  from the chosen atom to all other atoms in the lattice, the cohesive energy can be expressed in terms of three-dimensional lattice sums  $L_s \in \mathbb{R}_+$  multiplied by inverse powers of the nearest neighbor distance  $r_0$  as originally described by Lennard-Jones in 1924<sup>24,25</sup> and analyzed in detail by Borwein et al.<sup>26</sup>

For example, the  $(n, m)$  LJ potential, and, more specifically, the  $(12, 6)$  LJ potential with coefficients  $c_1 = \epsilon r_e^{12}$  ( $s_1 = 12$ ) and  $c_2 = -2\epsilon r_e^6$  ( $s_2 = 6$ ), becomes (in atomic units)

$$\begin{aligned} E_{\text{LJ}}(r_0) &= \frac{n m \epsilon}{2(n-m)} \left[ \frac{1}{n} L_n \left( \frac{r_e}{r_0} \right)^n - \frac{1}{m} L_m \left( \frac{r_e}{r_0} \right)^m \right] \\ &\stackrel{n=12}{=} \epsilon \left( \frac{r_e}{r_0} \right)^6 \left[ \frac{L_{12}}{2} \left( \frac{r_e}{r_0} \right)^6 - L_6 \right]. \end{aligned} \quad (4)$$

From eq 3, one easily obtains the corresponding analytical expressions for the volume dependent pressure  $P$  and the bulk modulus  $B$  of a lattice expressed in terms of lattice sums as<sup>19</sup>

$$\begin{aligned} P_{\text{ELJ}}(V) &= -\frac{\partial E_{\text{ELJ}}(V)}{\partial V} = \frac{1}{6V} \sum_{n=1}^{n_{\max}} s_n c_n L_{s_n} r_0^{-s_n} \\ &= \frac{1}{6} \sum_{n=1}^{n_{\max}} s_n f_L^{s_n/3} c_n L_{s_n} V^{-s_n/3-1} \end{aligned} \quad (5)$$

$$\begin{aligned} B_{\text{ELJ}}(V) &= V \frac{\partial^2 E_{\text{ELJ}}(V)}{\partial V^2} = \frac{1}{18V} \sum_{n=1}^{n_{\max}} s_n (s_n + 3) c_n L_{s_n} r_0^{-s_n} \\ &= \frac{1}{18} \sum_{n=1}^{n_{\max}} s_n (s_n + 3) f_L^{s_n/3} c_n L_{s_n} V^{-s_n/3-1}. \end{aligned} \quad (6)$$

These formulas clearly demonstrate the usefulness of an extended LJ potential as important solid-state properties can be calculated *analytically* to computer precision for any volume  $V$  or pressure  $P$  if the lattice sums are accurately known.

Working on the melting of argon, Herzfeld and Goepert-Mayer pointed out as early as in 1934 that lattice vibrations increase the equilibrium lattice distance and must therefore be

considered.<sup>27</sup> Corner<sup>28</sup> and Wallace<sup>29</sup> analyzed such lattice vibrational effects in more detail for the  $(n, 6)$  LJ potential and through approximations derived an analytical formula for the zero-point vibrational energy of the fcc lattice. Later, Nijboer and deWette analyzed lattice vibrations in  $k$ -space for the dynamic matrix for a face-centered cubic crystal with a varying lattice constant.<sup>30,31</sup> However, the corresponding lattice sums become rather complicated, and fast converging forms for the dynamic matrix for phonon dispersion are not available.

In this paper, we derive exact analytical expressions for the zero-point vibrational energy and corresponding anharmonicity correction to the cohesive energy and the lattice (mode) Grüneisen parameter within the Einstein approximation.<sup>32</sup> That is moving a single atom in the field of an ELJ potential, for the simple cubic (sc), body-centered cubic (bcc), or face centered cubic (fcc) lattices, including thermodynamic properties, and applying these formulas to various model systems for the rare gases from helium to the heaviest element in this group, oganesson. We also include in our discussion the more complicated hexagonal close-packed structure (hcp). As specific applications, we focus on the high-pressure range of helium and the fcc and hcp phases for argon, which are energetically very close, and discuss the limitations of the Einstein model. For the Grüneisen parameter, we investigate solid neon as an example where anharmonicity effects are large.

## METHODS

The total cohesive energy per atom,  $E_{\text{coh}}(V)$ , can be divided into static  $E_{\text{coh}}^{\text{stat}}(V)$  and dynamic  $E_{\text{coh}}^{\text{dyn}}(V)$  contributions, the latter resulting from zero-point vibrational motion:

$$E_{\text{coh}}(V) = E_{\text{coh}}^{\text{stat}}(V) + E_{\text{coh}}^{\text{dyn}}(V) \quad (7)$$

The total static contribution can be approximated within the many-body ansatz including two- and higher body contributions in the solid if the many-body expansion is converging fast.<sup>33</sup> We use translational symmetry to evaluate the most important two-body contribution through an ELJ potential,  $E_{\text{coh}}^{\text{stat}}(V) \cong E_{\text{ELJ}}(V)$ , and for the dynamic part,

$$E_{\text{coh}}^{\text{dyn}}(V) \cong E_{\text{ELJ}}^{\text{ZPVE}}(V) + E_{\text{ELJ}}^{\text{AZPVE}}(V) \quad (8)$$

We apply the Einstein approximation for a vibrating atom in the interacting ELJ field of all other atoms. Here  $E_{\text{ELJ}}^{\text{ZPVE}}(V)$  is the volume dependent zero-point vibrational energy (ZPVE) contribution within the harmonic oscillator approximation, and  $E_{\text{ELJ}}^{\text{AZPVE}}(V)$  is the corresponding anharmonicity correction (AZPVE). Although this treatment neglects important higher-body contributions and phonon dispersion and, for helium important quantum effects originating from the nuclear motion, analytical formulas derived in terms of eq 7 will provide us with some useful qualitative insight into solid-state properties. For a more accurate treatment which goes beyond this approximation, see ref 34, for example, where J/mol accuracy has been achieved for the cohesive energy of solid argon.

**Lattice Sums.** Lattice sums are of key importance in the work presented in this article, a field pioneered early on by Lennard-Jones.<sup>24,25</sup> Any expression in inverse powers of distances for interacting atoms in a lattice can be uniquely described by a three-dimensional lattice sum  $L_s$  (if convergent). For the case of the cubic lattices sc, bcc, and fcc we have<sup>26</sup>

$$\sum_{i=1}^{\infty} r_i^{-s} = L_s r_0^{-s} \quad (9)$$

**Table 1. Lennard-Jones Lattice Sums  $L_n$  with Respect to the Infinite Limit ( $L_\infty^{\text{sc}} = 6$ ,  $L_\infty^{\text{bcc}} = 8$ ,  $L_\infty^{\text{fcc}} = 12$ , and  $L_\infty^{\text{hpc}} = 12$ ) for  $n \in \mathbb{N}$  for the sc, bcc, fcc, and hpc Lattices<sup>a</sup>**

$n$	$L_n^{\text{sc}} - L_\infty^{\text{sc}}$	$L_n^{\text{bcc}} - L_\infty^{\text{bcc}}$	$L_n^{\text{fcc}} - L_\infty^{\text{fcc}}$	$L_n^{\text{hpc}} - L_\infty^{\text{hpc}}$
6	2.40192397482754	4.25366786729232	2.45392104374447	2.45489727784162
8	0.94580792722637	2.35519790840251	0.80193723137813	0.80282185280990
10	0.42611910253309	1.56440061535995	0.31124566547741	0.31189623381898
12	0.20214904504752	1.11418326807536	0.13188019654458	0.13229376909892
14	0.09818412571215	0.81677022848592	0.05899194435086	0.05922825506824
16	0.04826346958584	0.60625404754453	0.02735484401857	0.02747941930386

<sup>a</sup>For a more detailed table, see ref 40.

where the sum runs over all lattice points  $i$  in three dimensions located at distances  $r_i$  from a selected atom, is reduced to  $L_s$  multiplied by the nearest neighbor distance,  $r_0$  to the power of  $s$  ( $s > 3$  to ensure convergence of the lattice sum; otherwise appropriate expressions for the analytical continuation of conditionally convergent series have to be found as in the case for the Madelung constant<sup>35</sup>).

Analytical expressions for lattice sums  $L_s$  (also called Lennard-Jones–Ingham parameters) have a long history<sup>26,36</sup> and have been tabulated for a number of lattices with integer exponents ( $s \in \mathbb{N}$ ) by several authors.<sup>19,29,37–40</sup> Even for more complicated lattices such as hcp, expressions of the cohesive energy in terms of lattice sums have been formulated<sup>40</sup> based on the 1940 paper by Kane and Goepert-Mayer.<sup>41</sup> For the lattices considered in this work, we have the following lattice sums

$$L_s^{\text{sc}} = \sum_{i,j,k \in \mathbb{Z}}' [i^2 + j^2 + k^2]^{-s/2} \quad (10)$$

$$L_s^{\text{bcc}} = \sum_{i,j,k \in \mathbb{Z}}' \left[ i^2 + j^2 + k^2 - \frac{2}{3}(ij + ik + jk) \right]^{-s/2} \quad (11)$$

$$L_s^{\text{fcc}} = \sum_{i,j,k \in \mathbb{Z}}' [i^2 + j^2 + k^2 + ij + ik + jk]^{-s/2} \quad (12)$$

$$\begin{aligned} L_s^{\text{hpc}} = & \sum_{i,j,k \in \mathbb{Z}}' \left[ i^2 + j^2 + ij + \frac{8}{3}k^2 \right]^{-s/2} \\ & + \sum_{i,j,k \in \mathbb{Z}} \left[ \left( i + \frac{1}{3} \right)^2 + \left( j + \frac{1}{3} \right)^2 + \left( i + \frac{1}{3} \right) \left( j + \frac{1}{3} \right) \right. \\ & \left. + \frac{8}{3} \left( k + \frac{1}{2} \right)^2 \right]^{-s/2}. \end{aligned} \quad (13)$$

The notation  $\sum'$  implies that singularities in the sum at zero are avoided. Alternative decompositions to these expressions can also be found.<sup>40</sup> In fact, these lattice sums are functions of quadratic forms generated by its Gram matrix  $G_{ij} = \vec{b}_i^T \vec{b}_j$ , where  $\vec{b}_i$  are the generating basis vectors of the lattice.<sup>42</sup> A program to calculate these usually slow convergent lattice sums through various algorithms leading to fast converging series for real exponents  $s \in \mathbb{R}$ ,  $s > 3$  is freely available from our Web site,<sup>43</sup> and the lattice sums required for the formulas presented here for the LJ potential are given in Table 1. We have for the limit  $\lim_{s \rightarrow \infty} L_s = N_c$ , where  $N_c$  is the number of nearest neighbors in the crystal ( $N_c = 6$  for sc, 8 for bcc, and 12 for fcc and hcp), also

called the kissing number. The lattice sums (minus the kissing number for better comparison) are depicted in Figure 1.

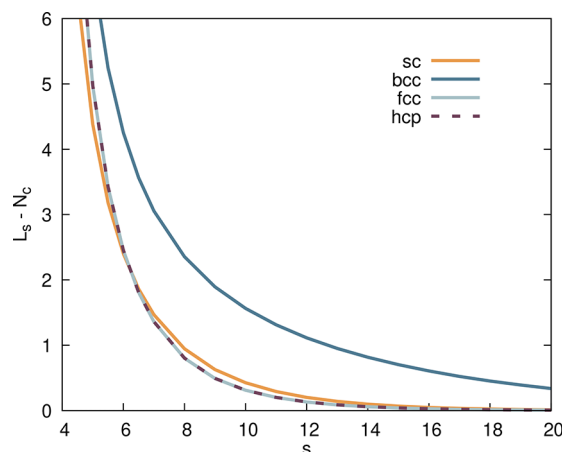


**Figure 1.** Lattice sums,  $L_s$  minus the kissing number,  $N_c = N_\infty$ , of sc, bcc, fcc, and hpc for a range of real exponents  $s$ . For details, see ref 40.

**Lattice Vibrations for the Cubic Lattices.** As we move an atom in the crystal field of all other atoms, we break translational symmetry. Hence we need to apply a 3D Taylor expansion first to find appropriate formulas for the harmonic and anharmonic contributions to the total energy, and introduce the lattice sums, eq 9, in a subsequent step. Within the Einstein (E) model each atom of mass  $M$  in the lattice is an independent 3D quantum harmonic oscillator;<sup>32</sup> i.e., all atoms oscillate with the same frequency  $\omega_E$ , whereas in the Debye model the atoms are assumed to be oscillating with their own frequencies and modes. For the zero-point vibrational energy contribution within the Einstein model, which neglects the vibrational coupling with neighboring atoms, we obtain a simple analytical formula for the three cubic lattices sc, bcc, and fcc analogous to the simple harmonic oscillator formula (atomic units are used throughout),

$$\begin{aligned} E_{\text{ELJ}}^{\text{ZPVE}} &= \frac{1}{2\sqrt{M}} (F_{xx}^{1/2} + F_{yy}^{1/2} + F_{zz}^{1/2}) \\ &= \frac{1}{2r_0} \sqrt{\frac{3}{M}} \left[ \sum_n s_n (s_n - 1) c_n L_{s_n+2} r_0^{-s_n} \right]^{1/2} \end{aligned} \quad (14)$$

where the second derivative matrix ( $F_{xy}$ ) denotes the harmonic force field. To obtain this expression, a selected atom is moved in an external ELJ field created by all the other atoms. The derivatives of the total energy with respect to the Cartesian coordinates of a moving atom in a crystal lattice up to fourth order, e.g.,  $F_{xyz} \dots = \partial^4 E / \partial x \partial y \partial z \dots$ , are detailed in the Appendix. For the cubic lattices, the Euclidean coordinate system ( $x, y, z$ ) is

chosen parallel to the crystal axes such that  $(F_{xy})$  is diagonal, and symmetry demands that  $F_{xx} = F_{yy} = F_{zz} = \text{Tr}(F)/3$ . We mention that Corner also used a Taylor expression, but in his classical treatment for the vibrational movement, he had to average over the angular part.<sup>28</sup>

The ZPVE for the  $(n, m)$  LJ potential, and more specifically, for the  $(12, 6)$  LJ potential with coefficients  $c_1 = \epsilon r_e^{12}$  ( $s_1 = 12$ ) and  $c_2 = -2\epsilon r_e^6$  ( $s_2 = 6$ ) becomes (in atomic units),

$$E_{\text{LJ}}^{\text{ZPVE}}(r_0) = \frac{1}{2r_e} \sqrt{\frac{3\epsilon}{M}} \sqrt{\frac{nm}{n-m}} \left( \frac{r_e}{r_0} \right)^{n/2+1} \times \left[ (n-1)L_{n+2} - (m-1)L_{m+2} \left( \frac{r_0}{r_e} \right)^{n-m} \right]^{1/2} \stackrel{n=12}{=} \frac{3}{r_e} \sqrt{\frac{\epsilon}{M}} \left( \frac{r_e}{r_0} \right)^7 \left[ 11L_{14} - 5L_8 \left( \frac{r_0}{r_e} \right)^6 \right]^{1/2} \quad (15)$$

This expression is identical with that of Corner for a  $(n, 6)$ -LJ potential.<sup>28</sup> The (harmonic) Einstein frequency,  $\omega_E = 2E_{\text{ELJ}}^{\text{ZPVE}}/3$ , becomes

$$\omega_E = \frac{1}{3\sqrt{M}} [3\text{Tr}(F)]^{1/2} = \frac{1}{r_0\sqrt{3M}} \left[ \sum_n s_n (s_n - 1) c_n L_{s_n+2} r_0^{-s_n} \right]^{1/2} \quad (16)$$

The anharmonicity correction is usually small and can be obtained from first-order perturbation theory. Since the third order term in the Taylor expansion around the origin is parity odd and the corresponding matrix elements thus equals zero, the anharmonicity correction is given by the corresponding expectation value (in Dirac notation) of the fourth order term (see eq 70 in the Appendix)

$$E_{\text{LJ}}^{\text{AZPVE}}(r_0) = \frac{3}{32Mr_0^2} \frac{(n+2)(n+1)(n-1)L_{n+4}r_e^{n-m} - (m+2)(m+1)(m-1)L_{m+4}r_0^{n-m}}{(n-1)L_{n+2}r_e^{n-m} - (m-1)L_{m+2}r_0^{n-m}} \stackrel{n=12}{=} \frac{21}{16M} \frac{20L_{10}r_0^6 - 143L_{16}r_e^6}{5L_8r_0^8 - 11L_{14}r_0^2r_e^6}. \quad (22)$$

This shows that, by using the Einstein model, compact analytical expressions can be obtained for the vibrational contributions for the ELJ potential. Since the quartic force-constants are all positive, the anharmonicity correction *increases* the zero-point vibrational energy in contrast to a diatomic molecule, where a nonzero (negative) cubic force constant becomes important in second-order perturbation, leading to a decrease in the vibrational levels and transitions.

By defining the following sums,

$$A_L(r_0) = r_0^{-2} \sum_n s_n (s_n - 1) c_n L_{s_n+2} r_0^{-s_n},$$

$$E^{\text{AZPVE}} = \frac{1}{24} \sum_{i=1}^{\infty} \sum_{n>3} c_n \langle \phi_0^E(\vec{r}) | (\vec{r} \cdot \vec{\nabla})^4 | \vec{r} - \vec{r}_i |^{-n} | \phi_0^E(\vec{r}) \rangle \quad (17)$$

where the corresponding ground state harmonic oscillator (HO) solutions for a vibrating atom in 3D space is given by the Hartree product

$$\phi_0^E(\vec{r}) = \phi_0^{\text{HO}}(x, \omega_E) \phi_0^{\text{HO}}(y, \omega_E) \phi_0^{\text{HO}}(z, \omega_E) \quad (18)$$

This is very much in the spirit of the perturbative treatment for the anharmonicity effects of a vibrating diatomic molecule. In first-order perturbation theory, we only have to consider two matrix elements in the Taylor expansion for the ground vibrational state (apart from the permutations in  $x$ ,  $y$ , and  $z$ ),  $\langle \psi_0^{\text{HO}}(x, \omega_E) | x^2 | \psi_0^{\text{HO}}(x, \omega_E) \rangle$ , and  $\langle \psi_0^{\text{HO}}(x, \omega_E) | x^4 | \psi_0^{\text{HO}}(x, \omega_E) \rangle$ , as all other quartic force constants with an odd number in one of the Cartesian coordinates of the moving atom are zero due to the crystal symmetry (and conveniently the cubic force field as well). The resulting anharmonic correction therefore becomes

$$E^{\text{AZPVE}} = \frac{3}{32M^2\omega_E^2} (F_{xxxx} + 2F_{xxyy}) \quad (19)$$

By using the results from the appendix, we obtain for an ELJ potential

$$E_{\text{ELJ}}^{\text{AZPVE}}(r_0) = \frac{1}{32M^2\omega_E^2} \sum_n (s_n + 2)(s_n + 1)s_n(s_n - 1)c_n L_{s_n+4} r_0^{-s_n-4} \quad (20)$$

and using eq 16

$$E_{\text{ELJ}}^{\text{AZPVE}}(r_0) = \frac{3}{32Mr_0^2} \frac{\sum_n (s_n + 2)(s_n + 1)s_n(s_n - 1)c_n L_{s_n+4} r_0^{-s_n}}{\sum_n s_n(s_n - 1)c_n L_{s_n+2} r_0^{-s_n}} \quad (21)$$

The AZPVE for the  $(n, m)$  LJ potential and, more specifically, for the  $(12, 6)$  LJ potential with coefficients  $c_1$  and  $c_2$  as defined above becomes (in atomic units)

$$B_L(r_0) = r_0^{-2} \sum_n (s_n + 2)s_n(s_n - 1)c_n L_{s_n+2} r_0^{-s_n}, \\ C_L(r_0) = r_0^{-2} \sum_n (s_n + 5)(s_n + 2)s_n(s_n - 1)c_n L_{s_n+2} r_0^{-s_n}, \\ D_L(r_0) = r_0^{-4} \sum_n (s_n + 2)(s_n + 1)s_n(s_n - 1)c_n L_{s_n+4} r_0^{-s_n}, \\ E_L(r_0) = r_0^{-4} \sum_n (s_n + 4)(s_n + 2)(s_n + 1)s_n(s_n - 1)c_n L_{s_n+4} r_0^{-s_n}, \\ F_L(r_0) = r_0^{-4} \sum_n (s_n + 7)(s_n + 4)(s_n + 2)(s_n + 1)s_n(s_n - 1)c_n L_{s_n+4} r_0^{-s_n}, \quad (23)$$

the volume/nearest neighbor distance expression for the ZPVE and anharmonicity corrections becomes

$$E_{\text{ELJ}}^{\text{ZPVE}}(r_0) = \frac{1}{2} \sqrt{\frac{3}{M}} A_L(r_0)^{1/2} \quad (24)$$

and

$$E_{\text{ELJ}}^{\text{AZPVE}}(r_0) = \frac{3}{32M} A_L(r_0)^{-1} D_L(r_0) \quad (25)$$

Analytical expressions for the vibrational pressure and bulk modulus contributions for these cubic lattice can now be obtained. We get, for the vibrational pressure,

$$P_{\text{ELJ}}^{\text{ZPVE}}(r_0) = \frac{1}{4V\sqrt{3M}} A_L(r_0)^{-1/2} B_L(r_0) \quad (26)$$

$$\begin{aligned} P_{\text{ELJ}}^{\text{AZPVE}}(r_0) \\ = \frac{1}{32VM} [A_L(r_0)^{-1} E_L(r_0) - A_L(r_0)^{-2} B_L(r_0) D_L(r_0)] \end{aligned} \quad (27)$$

and the bulk modulus,

$$\begin{aligned} B_{\text{ELJ}}^{\text{ZPVE}}(r_0) = \frac{1}{24V\sqrt{3M}} A_L(r_0)^{-1/2} [2C_L(r_0) \\ - A_L(r_0)^{-1} B_L(r_0)^2] \end{aligned} \quad (28)$$

$$\begin{aligned} B_{\text{ELJ}}^{\text{AZPVE}}(r_0) = \frac{1}{96VM} A_L(r_0)^{-1} \{E_L(r_0) - A_L(r_0)^{-1} \\ [2B_L(r_0)E_L(r_0) + C_L(r_0)D_L(r_0)] \\ + 2A_L(r_0)^{-2}D_L(r_0)B_L(r_0)^2\}. \end{aligned} \quad (29)$$

**Grüneisen Parameter.** An important parameter in the theory of the equation of state and thermal expansion of solids is the volume- (or pressure-) and temperature-dependent Grüneisen parameter  $\gamma(V, T)$ , which describes the effect of changing the volume of a lattice on its vibrational properties.<sup>44–47</sup> At the microscopic level, this parameter depends on the volume derivative of the phonon frequencies, and at  $T = 0$  K with wave vector  $\vec{k}$  and band index  $j$ , the dimensionless mode Grüneisen parameter becomes

$$\gamma_{\vec{k},j}(V) = -\frac{\partial(\ln \omega_{\vec{k},j}(V))}{\partial(\ln V)} \quad (30)$$

For the Einstein approximation, eq 30 simplifies to

$$\gamma_E(V) = -\frac{\partial(\ln \omega_E(V))}{\partial(\ln V)} \quad (31)$$

where we simply replaced the commonly used Debye frequency by the Einstein frequency. Using eqs 23, 24, and 26, we obtain the ELJ potential

$$\begin{aligned} \gamma_{E,h}^{\text{ELJ}}(r_0) &= -\frac{V}{E_{\text{ELJ}}^{\text{ZPVE}}(r_0)} \frac{\partial E_{\text{ELJ}}^{\text{ZPVE}}(r_0)}{\partial V} = V \frac{P_{\text{ELJ}}^{\text{ZPVE}}(r_0)}{E_{\text{ELJ}}^{\text{ZPVE}}(r_0)} \\ &= \frac{B_L(r_0)}{6A_L(r_0)} \end{aligned} \quad (32)$$

There is no mass dependence in  $\gamma_{E,h}^{\text{ELJ}}(r_0)$ . The Grüneisen parameter for the  $(n, m)$  LJ potential, and more specifically, the  $(12, 6)$  LJ potential with our coefficients  $c_1$  and  $c_2$  as defined above becomes (in atomic units),

$$\begin{aligned} \gamma_{E,h}^{\text{LJ}}(r_0) \\ = \frac{1}{6} \frac{(n+2)(n-1)L_{n+2} \left(\frac{r_e}{r_0}\right)^{n-m} - (m+2)(m-1)L_{m+2}}{(n-1)L_{n+2} \left(\frac{r_e}{r_0}\right)^{n-m} - (m-1)L_{m+2}} \\ \stackrel{n=12}{=} \frac{77L_{14}r_e^6 - 20L_8r_0^6}{33L_{14}r_e^6 - 15L_8r_0^6} = \frac{77L_{14}V_e^2 - 20L_8V^2}{33L_{14}V_e^2 - 15L_8V^2} \end{aligned} \quad (33)$$

where  $V_e$  is the volume at nearest neighbor distance  $r_0 = r_e$ . The simplicity of this analytical formula demonstrates the beauty of the Einstein model. In a similar way, one can derive the anharmonicity contribution to the mode Grüneisen parameter by the substitution  $E_{\text{ELJ}}^{\text{ZPVE}}(r_0) \rightarrow E_{\text{ELJ}}^{\text{ZPVE}}(r_0) + E_{\text{ELJ}}^{\text{AZPVE}}(r_0)$ ,

$$\gamma_{E,h+ah}^{\text{ELJ}}(r_0) = V \frac{P_{\text{ELJ}}^{\text{ZPVE}}(r_0) + P_{\text{ELJ}}^{\text{AZPVE}}(r_0)}{E_{\text{ELJ}}^{\text{ZPVE}}(r_0) + E_{\text{ELJ}}^{\text{AZPVE}}(r_0)} \quad (34)$$

leading to a more complicated mass-dependent expression.

**The Hexagonal Close-Packed Structure.** Like fcc, the hcp lattice is a close-packed structure and often lies energetically very close to fcc. For the hard-sphere model the fcc and hcp packing densities are identical, as are any mixed fcc/hcp Barlow packings.<sup>48</sup> We remember that a cubic lattice is a lattice whose points lie at positions  $(n_1, n_2, n_3)$  in the Cartesian three-space, where  $n_i$  are integers. Unlike fcc, however, the hcp lattice is not cubic and is not a Bravais lattice but instead belongs to the  $D_{6h}$  point group. Although it has inversion symmetry, symmetry breaking occurs in the force field resulting in a lifting of the degeneracy of the Einstein frequencies. Hence, we lose the high symmetry compared to the three cubic lattices. This results in a far more complicated expression for the hcp compared to the fcc lattice sum, i.e., compare eqs 10–12 with eq 13, which has been resolved in terms of fast converging series only very recently by our group.<sup>40</sup>

The hcp lattice can be seen as a hexagonal Bravais lattice with lattice vectors  $\vec{a}_1 = \frac{a}{2}\hat{x} - \frac{\sqrt{3}a}{2}\hat{y}$ ,  $\vec{a}_2 = \frac{a}{2}\hat{x} + \frac{\sqrt{3}a}{2}\hat{y}$ ,  $\vec{a}_3 = \hat{z}$ , but with two atoms located at positions  $\vec{r}_1^T = (0, 0, 0)$  and  $\vec{r}_2^T = (2/3, 1/3, 1/2)$ . Since each atom is experiencing exactly the same field from all other surrounding atoms in the bulk system, we only need to consider the summation over the many-body contributions from the atom placed at the origin for the cohesive energy. This implies that both atoms give the same diagonal 3D force field and the same set of Einstein frequencies. However, from the lattice vectors and the atom located at the origin, it is clear that the vibration parallel to the hexagonal plane ( $h$ ) axis will differ from the vibrations perpendicular to it ( $c$ ). Thus, we get for the diagonal force constants  $F_{xx} = F_{yy} \neq F_{zz}$  and the corresponding three Einstein frequencies  $\omega_1^h = \omega_2^h \neq \omega_3^c$ . Even so, we have relations between the different force constant for the hcp lattice as detailed by Wallace,<sup>29</sup> unfortunately for the Einstein frequency, we have a sum of square-root terms for the force constants. Therefore, the relations found for the cubic lattices cannot be applied anymore for the hcp structure. Fortunately, it turns out that the difference  $\Delta\omega = \omega_2^h - \omega_3^c$  is very small (on the order of 0.01 cm<sup>-1</sup> for argon) such that we can safely set  $F_{xx} \approx F_{zz}$  and obtain to a very good approximation for hcp the same expression as in (14) with the corresponding hcp lattice sums. This also holds for very small volumes (high pressures) as confirmed by numerical calculations carried out with our program SAMBA.<sup>49</sup> The fact that eq 14 works is not

Table 2. (12, 6) LJ and ELJ Properties for the fcc Lattices of the Rare Gases at Minimum Energy<sup>a</sup>

isotope	$-\epsilon$	$E^{\text{stat}}$	$E^{\text{ZPVE}}$	$E^{\text{AZPVE}}$	$r_e$	$r^{\text{infl}}$	$r_0^{\text{min}}$	$r_0^{\text{ZPVE}}$	$r_0^{\text{infl}}$	$r_0^{\text{crit}}$
LJ										
<sup>3</sup> He	-34.8	-299.8	462.3	153.2	2.9676	3.2901	2.8822	(3.3508)	3.1955	3.3508
<sup>4</sup> He	-34.8	-299.8	401.3	115.4	2.9676	3.2901	2.8822	(3.3508)	3.1955	3.3508
<sup>20</sup> Ne	-133.5	-1149.4	337.7	21.3	3.0895	3.4252	3.0006	3.1250	3.3267	3.4884
<sup>40</sup> Ar	-453.2	-3902.5	361.4	7.2	3.7618	4.1706	3.6536	3.6975	4.0507	4.2476
<sup>84</sup> Kr	-636.1	-5477.3	276.8	3.0	4.0158	4.4523	3.9003	3.9255	4.3242	4.5344
<sup>132</sup> Xe	-894.0	-7697.1	240.9	1.6	4.3630	4.8372	4.2375	4.2543	4.6980	4.9264
<sup>222</sup> Rn	-1282.2	-11040	219.2	0.9	4.4270	4.9081	4.2997	4.3104	4.7670	4.9986
<sup>294</sup> Og	-2844.3	-24490	290.1	0.7	4.3290	4.7995	4.2045	4.2108	4.6614	4.8880
ELJ										
<sup>3</sup> He	-34.9	-258.1	432.0	113.9	2.9676	3.2906	2.9112	(3.3530)	3.2322	3.3530
<sup>4</sup> He	-34.9	-258.1	375.0	85.8	2.9676	3.2906	2.9112	(3.3530)	3.2322	3.3530
<sup>20</sup> Ne	-132.2	-1040.7	328.7	17.8	3.0930	3.4167	3.0278	3.1538	3.3501	3.4768
<sup>40</sup> Ar	-441.8	-3470.0	346.7	5.5	3.7782	4.1731	3.7004	3.7430	4.0958	4.2460
<sup>84</sup> Kr	-636.1	-4683.6	266.6	2.2	4.0157	4.4381	3.9346	3.9584	4.3577	4.5156
<sup>132</sup> Xe	-894.3	-6844.8	233.8	1.2	4.3616	4.8126	4.2782	4.2941	4.7309	4.8943
<sup>222</sup> Rn	-1212.9	-9665.3	202.9	0.6	4.4407	4.9153	4.3420	4.3520	4.8235	5.0004
<sup>294</sup> Og	-2853.6	-22482	258.1	0.4	4.3138	4.8259	4.1957	4.2011	4.7122	4.9256

<sup>a</sup> Binding energies  $-\epsilon$ , cohesive energies  $E^{\text{stat}}$ , zero-point vibrational energies (ZPVE)  $E^{\text{ZPVE}}$ , and anharmonicity corrections  $E^{\text{AZPVE}}$  in [ $\mu\text{Ha}$ ] at  $r_0^{\text{min}}$ . Equilibrium distances  $r_e$  of the diatomic, nearest neighbor distance of the solid  $r_0^{\text{min}}$ , ZPVE-corrected nearest neighbor distance  $r_0^{\text{ZPVE}}$ , critical distance  $r_0^{\text{crit}}$ , and inflection point  $r_0^{\text{infl}}$  in [ $\text{\AA}$ ]. Atomic masses  $M$  used (in [amu]) are 3.016 and 4.003 for <sup>3</sup>He and <sup>4</sup>He respectively, 19.992 for <sup>20</sup>Ne, 39.962 for <sup>40</sup>Ar, 83.912 for <sup>84</sup>Kr, 131.904 for <sup>132</sup>Xe, 222.018 for <sup>222</sup>Rn, and 294.0 for <sup>294</sup>Og. Binding energies and equilibrium distances for the (12, 6) LJ potential are taken from the literature.<sup>22,57-59</sup> The ELJ potential parameters are from He (this work), Ne,<sup>55</sup> Ar,<sup>34</sup> Kr,<sup>60</sup> Xe,<sup>60</sup> Rn,<sup>61</sup> and Og.<sup>62</sup>

surprising as we can use Corner's approximate treatment of vibrational motions applied to the hcp lattice.<sup>28</sup>

Analyzing the higher derivatives for the hcp force field we obtain the symmetry relations for the quartic force constants  $F_{xxxx} = F_{yyyy} \neq F_{zzzz}$  and  $F_{xxzz} = F_{yyzz} \neq F_{xyyy}$ , as discussed in detail by Wallace.<sup>29</sup> Again we see to a good approximation that  $F_{xxxx} \approx F_{zzzz}$ , but see larger differences for the mixed contributions in our numerical calculations. Fortunately,  $F_{zzzz} \gg F_{xxzz}$ , and therefore, the AZPVE expression in eq 19 is applicable to a good approximation for the hcp lattice as well. For example, comparing both equations with numerical simulations for hcp argon at a volume set at 24  $\text{cm}^3/\text{mol}$  (nearest neighbor distance of 3.8341  $\text{\AA}$  close to the equilibrium distance), we obtain from numerical force field calculations the Einstein frequencies  $\omega^h = 33.152$  and  $\omega^c = 33.141 \text{ cm}^{-1}$  and the ZPVE and AZPVE corrections of 49.7230 and  $1.7758 \text{ cm}^{-1}$  respectively. This compares well with the ZPVE and AZPVE contributions from eqs 14 and 19 of 49.7230 and  $1.7732 \text{ cm}^{-1}$  respectively, where the latter small difference could come from numerical inaccuracies.

**Thermodynamics.** The thermodynamics of the solid state using the LJ potential has been reviewed by Anderson, containing many useful formulas.<sup>50</sup> The finite temperature contributions to the entropy and free energy may now also be expressed in terms of the lattice sums, using the expression for the Einstein frequency and the Boltzmann distribution. We start from the partition function for a single harmonic oscillator with frequency  $\omega_b$

$$Z_i = \frac{e^{-\beta\omega_b/2}}{1 - e^{-\beta\omega_b}} \quad (35)$$

with  $\beta = 1/k_B T$ ,  $T$  being the temperature and  $k_B$  the Boltzmann constant converting the units of Kelvin to the desired energy unit. From this, we get the phonon free energy for  $N$  vibrating atoms,  $F_{\text{vib}} = -k_B T \ln Z$ ,

$$F_{\text{vib}} = \frac{1}{2} \sum_i^{3N} \omega_i + \beta^{-1} \sum_i^{3N} \ln(1 - e^{-\beta\omega_i}) \quad (36)$$

which contains the zero-point vibrational contribution and the phonon entropy  $S = k_B T \partial(\ln Z) / \partial T + k_B (\ln Z)$ ,

$$S_{\text{vib}} = k_B \sum_i^{3N} \left[ -\ln(1 - e^{-\beta\omega_i}) - \frac{\beta\omega_i}{1 - e^{-\beta\omega_i}} \right] \quad (37)$$

This expression trivially shows that for  $T \rightarrow 0$  there is, aside the residual entropy, no entropy difference due to zero-point vibration between the lattices. For the Einstein approximation, we obtain from eq 36 the relation

$$F_{\text{vib}} = \frac{3}{2} \omega_E + 3\beta^{-1} \ln(1 - e^{-\beta\omega_E}) \quad (38)$$

and

$$S_{\text{vib}} = 3k_B \left[ -\ln(1 - e^{-\beta\omega_E}) - \frac{\beta\omega_E}{1 - e^{-\beta\omega_E}} \right] \quad (39)$$

We obtain the following equation for the specific heat at constant volume ( $F = E - TS$ )

$$C_V = \left( \frac{\partial E}{\partial T} \right)_V = \frac{3}{4} k_B (\beta\omega_E)^2 \left[ \frac{e^{\beta\omega_E}}{(e^{\beta\omega_E} - 1)^2} \right] \quad (40)$$

## RESULTS AND DISCUSSION

In this section, we apply our derived formulas for the LJ and ELJ potentials to the rare gas bulk phases of which the LJ potential already has a long history in the treatment of bulk systems.<sup>19,51-53</sup> Beside the simplicity of this model, for which we shall highlight the limitations, especially for a quantum system such as bulk helium, it offers qualitative yet valuable insight into bulk properties. Furthermore, these analytical

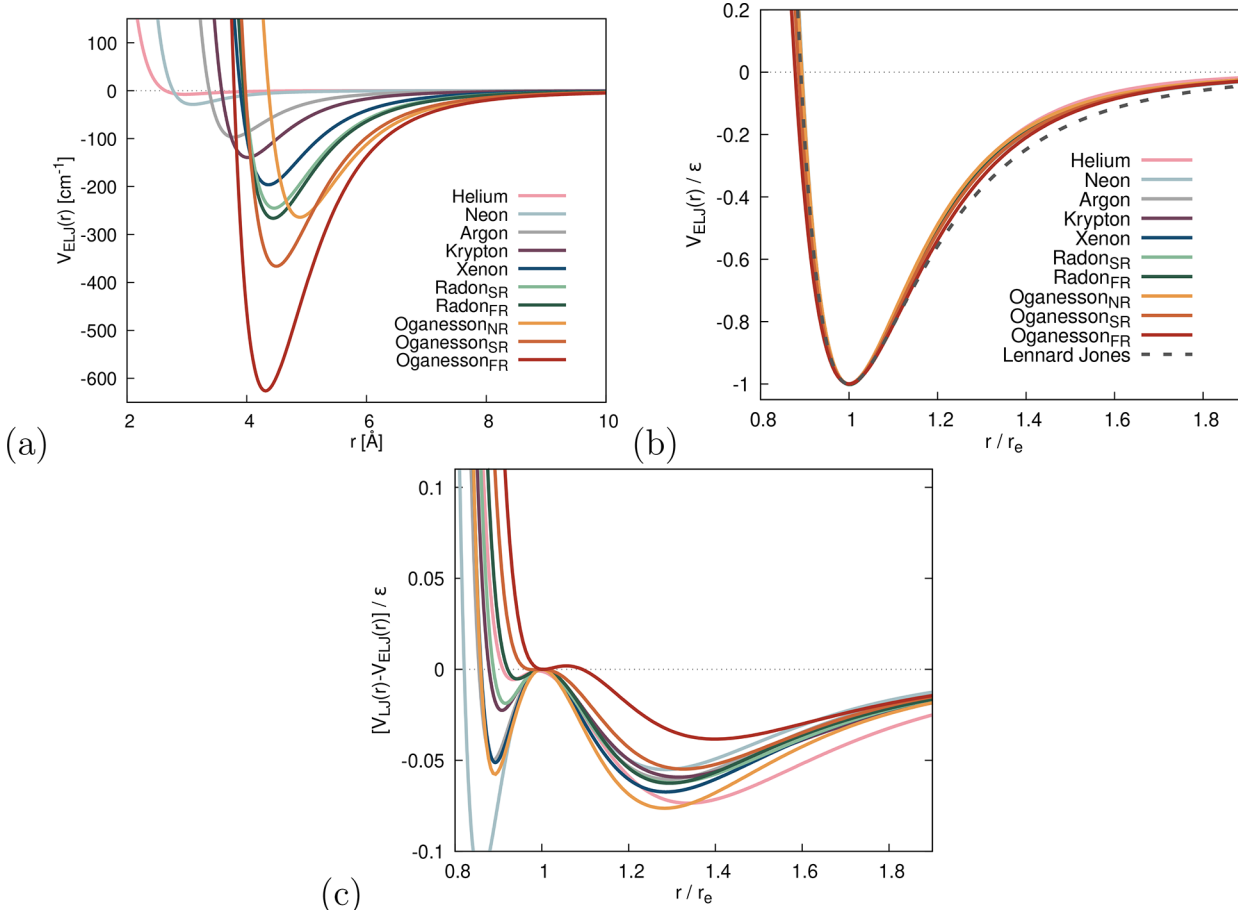


**Figure 2.** (a) ELJ potentials of the noble gases, including potentials of Rn and Og at different levels of relativistic theory (NR, nonrelativistic; SR, scalar relativistic; FR, fully relativistic (X2C)). (b) All potentials rescaled to a potential with  $r_e = 1$  and  $\epsilon = 1$ . In gray is given the (12, 6) LJ potential. (c) Difference between the LJ and ELJ potentials with  $r_e = 1$ ,  $\epsilon = 1$ , and  $\Delta V(r) = V_{LJ}(r) - V_{ELJ}(r)$ .

formulas serve as a first good initial estimate of how important vibrational effects are for bulk quantities such as the equation of state. They also point toward further improvements like inclusion of higher body forces, phonon dispersion, and, in the case of helium, dynamic effects to achieve better agreement with experimental observations. It should be borne in mind, however, that the rare gas solids represent a special case as the many-body expansion of the interaction energy converges reasonably fast with increasing  $n$ -body force, even at higher pressures.<sup>33,34,54–56</sup> The results are collected in Table 2, and the potential curves used are shown and analyzed in Figure 2a–c.

**The Equilibrium Nearest Neighbor Distance and Cohesive Energy of the Rare Gas Solids.** From the condition  $\partial E_{ELJ}(r_0)/\partial r_0 = 0$ , we derive the minimum nearest neighbor distance  $r_0^{\min}$  of the atoms in the solid described by an ELJ potential. In the case of a general  $(n, m)$  LJ potential, we obtain a simple relationship between the equilibrium distance  $r_e$  of the diatomic and the lattice  $r_0^{\min}$  value,<sup>19</sup>

$$r_0^{\min} = \left( \frac{L_n}{L_m} \right)^{1/(n-m)} r_e \quad (41)$$

As for  $n > m$ , we have  $L_n < L_m$ ; for a specific lattice,<sup>40</sup> we have  $r_0^{\min} < r_e$ . The same inequality holds for the ELJ potentials for the rare gases as the values in Table 2 show and is due to the fact that the lattice summation introduces attractive forces originating from

non-nearest neighbors, causing a bond contraction compared to the diatomic.

Using our analytical expressions, we can determine the nearest neighbor distance for an ELJ potential including zero-point vibration. Table 2 shows that vibrational effects increase the nearest neighbor distance in the solid,  $r_0^{ZPVE} > r_0^{\min}$ , as pointed out earlier by accurate ab initio calculations.<sup>34,60–63</sup> For example, the total cohesive energy for a (12, 6) LJ potential including harmonic vibrational contributions within the Einstein approximation from eqs 3 and 14 becomes

$$\begin{aligned} E_{LJ}^T(r_0) &= E_{LJ}^{\text{stat}}(r_0) + E_{LJ}^{\text{ZPVE}}(r_0) \\ &= \frac{1}{2} (c_6 L_6 r_0^{-6} + c_{12} L_{12} r_0^{-12}) \\ &\quad + \frac{3}{\sqrt{2M}} r_0^{-7} (5c_6 L_6 r_0^6 + 22c_{12} L_{12})^{1/2}. \end{aligned} \quad (42)$$

For the following we omit the label “stat” for the static cohesive energy. For the minimum  $\partial E_{LJ}^T(r_0)/\partial r_0 = 0$ , we get, after some algebraic manipulations, an 11th order polynomial in  $x = r_0^{-2}$ ,

$$a_0 + a_3 x^3 + a_5 x^5 + a_6 x^6 + a_8 x^8 + a_9 x^9 + a_{11} x^{11} = 0 \quad (43)$$

with the coefficients  $a_0 = 44\epsilon L_{12}^2 L_{14}$ ,  $a_3 = -4\epsilon r_e^{-6} L_{12} (22L_6 L_{14} + 5L_8 L_{12})$ ,  $a_5 = -5929M^{-1} r_e^{-12} L_{14}^2$ ,  $a_6 = 4\epsilon r_e^{-12} L_6 (11L_6 L_{14} + 10L_8 L_{12})$ ,  $a_8 = 3080M^{-1} r_e^{-18} L_8 L_{14}$ ,

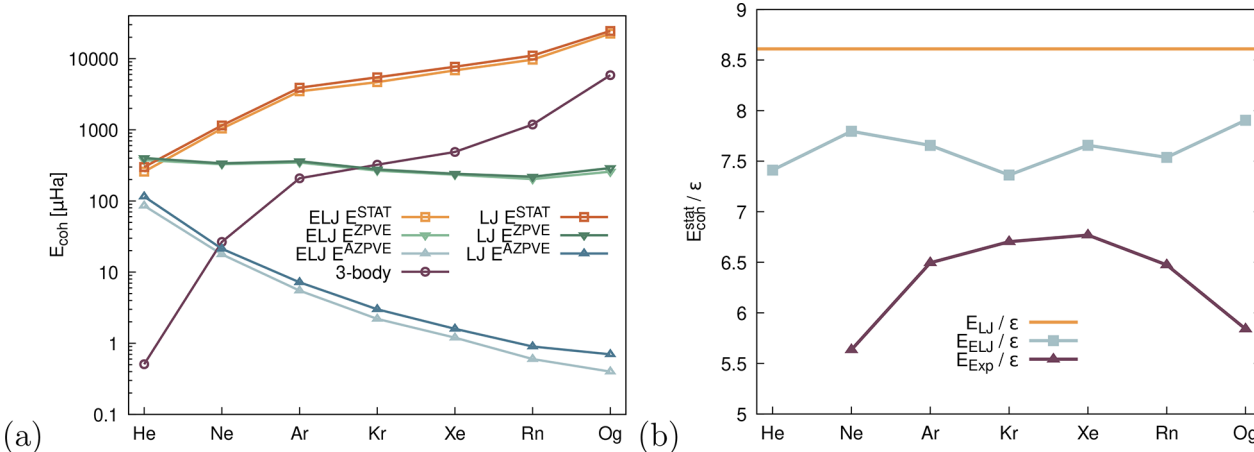


**Figure 3.** (a) Trends in cohesive energy contributions for  $E^{stat}$ ,  $E^{ZPVE}$ ,  $E^{AZPVE}$ , and  $E^{(3)}$  (in  $\mu\text{Ha}$ ) shown at a logarithmic scale for all the rare gases. The values in Table 2 were chosen, and for helium the  ${}^4\text{He}$  isotope was selected. The three-body contribution  $E^{(3)}$  was taken from ref 66, for Ne to Xe, and from ref 62, for Rn and Og. For He, the program Samba was used, and the three-body potential of Cencek, Patkowski and Szalewicz was taken<sup>67</sup> at the equilibrium distance  $r_e$  for the dimer listed in Table 2. (b) Ratio between the two-body ELJ cohesive energy  $E_{ELJ}$  and the binding energy  $-\epsilon$  of the diatomic molecule (values taken from Table 2), and ratio for the best available cohesive energies<sup>62–66</sup>  $E_{coh}$  and  $\epsilon$ . The ideal LJ ratio is shown as a straight line.

$a_9 = -20\epsilon r_e^{-18}L_6^2L_8$ , and  $a_{11} = -400M^{-1}r_e^{-24}L_8^2$ . The problem is then reduced to finding the zeros of the polynomial (43). There is no trivial solution except for  $M \rightarrow \infty$ , which yields just  $r_0^{\min}$  for the minimum structure of the lattice, and the polynomial has exactly one real solution. For a finite mass, the polynomial needs to be evaluated case by case. For all the rare gas solids, the polynomial has three real solutions, and we find the second root to be the physical one. A similar expression can be obtained if the anharmonicity correction is added.

Using eq 41 for (4), we obtain a relationship for the cohesive energy at  $r_0^{\min}$  in terms of the binding energy of the diatomic molecule and lattice sums,

$$E_{LJ}(r_0^{\min}) = \epsilon \frac{nm}{2(n-m)} \left[ \frac{L_n}{n} \left( \frac{L_m}{L_n} \right)^{n/(n-m)} - \frac{L_m}{m} \left( \frac{L_m}{L_n} \right)^{n/(n-m)} \right] \\ \stackrel{n=12}{=} -\epsilon \frac{L_6^2}{2L_{12}} \quad (44)$$

Parts a and b of Figure 3, show trends in cohesive energy contributions and a comparison between the LJ and ELJ potentials along the row of the rare gas solids. For the fcc lattice we have  $L_6^2/2L_{12} = 8.6102$ .<sup>19</sup> The ratios  $-E_{ELJ}(r_0^{\min})/\epsilon$  for the ELJ potential as well as with respect to the experimental or best theoretical values for the rare gas lattices are shown in Figure 3b. There are two important messages we can deduce from this figure. First, the ELJ potential gives lower cohesive energies compared to the (12, 6) LJ potential, and the ratio  $E_{ELJ}/\epsilon$  varies slightly between 7.36 (Kr) and 7.90 (Og) compared to the LJ ideal value of 8.6102. Second, if we take the best available cohesive energy values for the rare gases to obtain the ratio  $E_{coh}/\epsilon$ ,<sup>62–66</sup> we see that zero-point vibrational effects lead to larger deviations for the lighter rare gas elements and the three-body effects to larger deviations for the heavier ones.

Table 2 shows properties for the fcc phase of the rare gas solids obtained by using both a (12, 6) LJ and an ELJ potential with the values for the lattice sums  $L_n$  published recently.<sup>40</sup> The corresponding potential curves are drawn in Figure 2a, which show the very weak bonding for the lightest element, helium, and the relatively strong bonding for the heaviest element in this

group, oganesson. As can be seen from Figure 2a, the unusually large cohesive energy of the heaviest known element in the periodic table is due to relativistic effects,<sup>62,68,69</sup> which, despite the very large three-body contribution, results in a melting point above room temperature for oganesson.<sup>70</sup>

Concerning vibrational effects, we obtain a slow decrease in the ZPVE with increasing mass, gradually becoming less important compared to the static part of the cohesive energy. Oganesson is exceptional, since the increase in the cohesive energy and decrease in the bond distance, both due to relativistic effects, lead to a larger vibrational contribution compared to radon despite the larger mass.<sup>62</sup> In contrast, anharmonicity effects diminish rather fast with increasing  $Z$ ; see Figure 3a. This can be understood from eqs 14 and 21. For the ZPVE, we have  $E_{LJ/ELJ}^{ZPVE} \propto r_0^{-1} \sqrt{\epsilon/M}$ . As  $\epsilon$ ,  $M$ , and  $r_0$  increase down the group in the periodic table we have a compensating effect and a small net decrease in the Einstein frequency. For the anharmonic contribution, however, we have  $E_{LJ/ELJ}^{AZPVE} \propto r_0^{-2}M^{-1}$  leading to a much faster decrease in  $E_{LJ/ELJ}^{AZPVE}$  with increasing mass and distance  $r_0^{\min}$ .

To compare to experimental values we take solid argon as an example. The experimental nearest neighbor distance is 3.7560 Å,<sup>71</sup> and the cohesive energy  $-2941(4)$   $\mu\text{Ha}$ ,<sup>65</sup> in good agreement with the ELJ values of  $E_{ELJ} + E_{ELJ}^{ZPVE} + E_{ELJ}^{AZPVE} = -3118$   $\mu\text{Ha}$ . If we take the optimized  $r_0^{\min}$  distance instead, we obtain a similar value of 3134  $\mu\text{Ha}$ . The (12, 6) LJ potential with  $-3534$   $\mu\text{Ha}$  clearly overestimates the cohesive energy. The remaining error for the ELJ potential lies mainly in the missing three-body effect. For a detailed analysis of the rare gas solids, see refs 34 and 60–63. For comparison, we include three-body contributions from the literature in Figure 3, which shows that these effects become increasingly important with increasing nuclear charge and polarizability of the rare gas atom.<sup>72</sup>

Figure 2b compares the ELJ potentials by scaling both the equilibrium distance and the binding energy to unity. They all show a very similar functional form, the differences being barely visible on this graph. This suggests that, to a reasonable approximation, we can use the same analytical form for  $\epsilon^{-1}E_{ELJ}(r/r_e)$ , which needs to be further investigated for the solid state properties of the rare gases. Figure 2c shows the

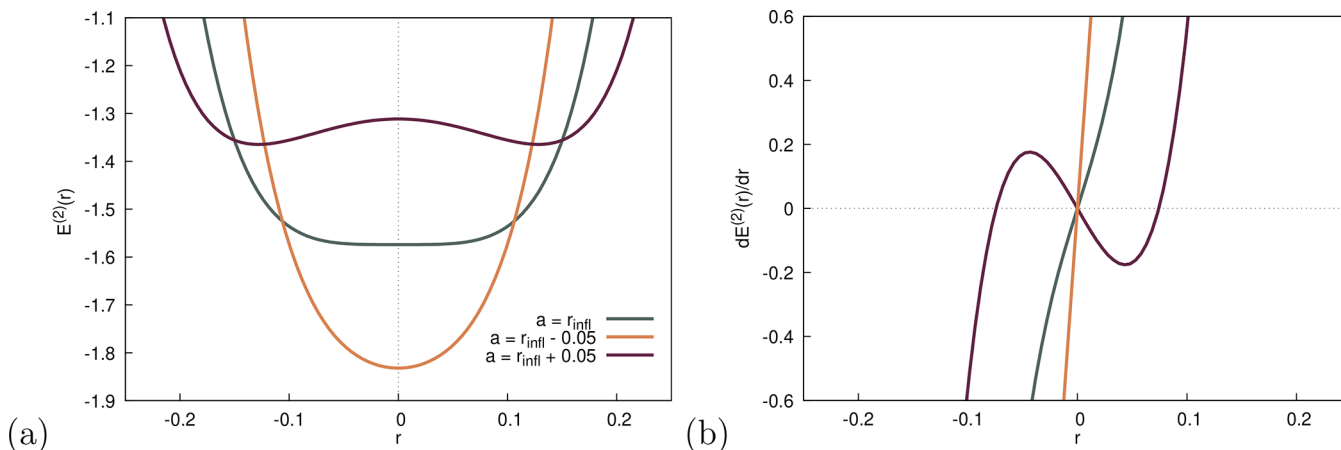


**Figure 4.** (a) LJ potential experienced by an atom confined by two other atoms to the left and right and separated by a distance of  $2a$  resulting in a total interaction energy of  $E_{\text{LJ}}(r) = (r + a)^{-12} - 2(r + a)^{-6} + (r - a)^{-12} - 2(r - a)^{-6}$ . The parameter used is  $a = r_{\text{infl}} + 0.05$ ,  $a = r_{\text{infl}}$ , or  $a = r_{\text{infl}} - 0.05$  (the inflection distance which is equal to the critical distance for a 1-dimensional chain). (b) Corresponding effective on-site forces.

difference between these curves and the standard (12, 6) LJ potential. We see that the LJ potential overbinds in the long-range, but becomes too repulsive in the short-range, which will have consequences for the pressure–volume and bulk modulus–volume equations of states as we shall see below. However, before we proceed with the discussion of three of the rare gas solids, helium, neon, and argon, we shall briefly discuss the analytical expressions for the critical points for the LJ and the ELJ potentials and their relevance for the solid state.

**Critical Points for the Extended Lennard-Jones Potential Energy Curves.** Multiple critical points, which in a strict mathematical sense are points on the function where the first or higher-order derivatives are equal to zero or where the function or derivative is discontinuous, for the ELJ potential can be identified. The first critical point is at the nearest neighbor distance  $r_0^{\text{min}}$ , where the pressure is zero,  $P = \partial E^{\text{coh}}(r_0)/\partial r_0 = 0$ . Expansion beyond the nearest neighbor distance into the region of negative pressure,  $r > r_0^{\text{min}}$ , is achieved by adding thermal pressure through the Boltzmann term, which keeps the pressure positive. The negative pressure range has however been used, for example, to theoretically analyze the metal-to-nonmetal transition in expanded fluid mercury.<sup>73</sup>

A second critical point lies at the distance where  $\partial^2 E^{\text{coh}}(r_0)/\partial r_0^2 = 0$ , referred to as the cohesive energy inflection point

$$r_0^{\text{infl}} = \left[ \frac{(n+1)L_n}{(m+1)L_m} \right]^{1/(n-m)} \quad r_e = \left[ \frac{(n+1)}{(m+1)} \right]^{1/(n-m)} r_0^{\text{min}} \\ = \left[ \frac{L_n}{L_m} \right]^{1/(n-m)} r^{\text{infl}} \quad (45)$$

where  $r^{\text{infl}}$  is the inflection point of the (12, 6) LJ potential defined in eq 1. For the (12, 6) LJ potential we have  $r_0^{\text{infl}} = 1.07679r_e = 1.10868r_0^{\text{min}}$ . The restoring forces decrease with increasing deviations from equilibrium, and at the inflection point, the bulk modulus becomes zero, indicating that the compressibility becomes infinitely high, alike a gas at very low pressure. Even though the lattice symmetry is maintained when moving along the cohesive energy curve, this hints that the inflection point can be used as a qualitative measure for symmetry breaking in the solid, resulting in a phase transition into the liquid or gas phase.<sup>74,75</sup>

Symmetry breaking occurs when one or more atoms in the lattice or unit cell move to positions where the lattice symmetry is not conserved, in contrast to expansion or compression of all atoms simultaneously of which the energy is given by the cohesive energy curve for the specific lattice symmetry. A good example for symmetry breaking is the so-called Peierls distortion (Jahn–Teller effect).<sup>76,77</sup> A local form of symmetry breaking happens when the Einstein frequency becomes zero and the square root in eq 14 or 15 vanishes. This form of symmetry breaking was already discussed qualitatively for helium in 1955 by Houton<sup>52,78</sup> and occurs at a distance of

$$r_0^{\text{crit}} = \left[ \frac{(n-1)}{(m-1)} \frac{L_{n+2}}{L_{m+2}} \right]^{1/(n-m)} r_e \\ = \left[ \frac{(n-1)}{(m-1)} \frac{L_{n+2}L_m}{L_{m+2}L_n} \right]^{1/(n-m)} r_0^{\text{min}} \quad (46)$$

For the (12, 6) LJ potential,  $r_0^{\text{crit}} = 1.12912 r_e = 1.16257 r_0^{\text{min}}$ . Note that both eq 45 and eq 46 are not mass dependent. At expansion beyond  $r_0^{\text{crit}}$ , a double minimum for the internal energy of the atom is formed, causing the atom to move away from the equilibrium distance and consequently the lattice locally distorts, breaking the symmetry of the bulk system. Yet, this simplified Einstein picture involves only the movement of one atom in the field of all other atoms which are kept at lattice symmetry points. If we allow all atoms in the solid to move, the point where symmetry breaks,  $r_0^{\text{sb}}$ , lies below this Einstein estimate,  $r_0^{\text{sb}} < r_0^{\text{crit}}$ , and perhaps also below the inflection point for which we have  $r_0^{\text{infl}} < r_0^{\text{crit}}$ .

We briefly consider the inflection point and critical distance for close-packed structures in one and two dimensions for a LJ potential as they serve as good models for symmetry breaking effects in solids. The expressions for the cohesive energy in eq 4, the inflection point, eq 45, and critical distance, eq 46, remain unchanged except that we have to substitute the 3D lattice sums  $L_n^{3D}$  for the corresponding 1D or 2D ones. For a one-dimensional chain, these are related to the well-known Riemann  $\zeta$  function, i.e.,  $L_n^{1D} = 2\zeta(n)$  with the number of nearest neighbors  $L_{\infty}^{1D} = 2$ . Thus for the (12, 6) LJ potential, we have  $\zeta(6) = \pi^6/945$ ,  $\zeta(8) = \pi^8/9450$ ,  $\zeta(12) = 691\pi^{12}/638512875$  and  $\zeta(14) = 2\pi^{14}/18243225$ . We obtain  $r_0^{1D,\text{infl}} = 1.10556r_e$  and  $r_0^{1D,\text{crit}} = 1.13967r_e$ . However, moving an atom in-between only two

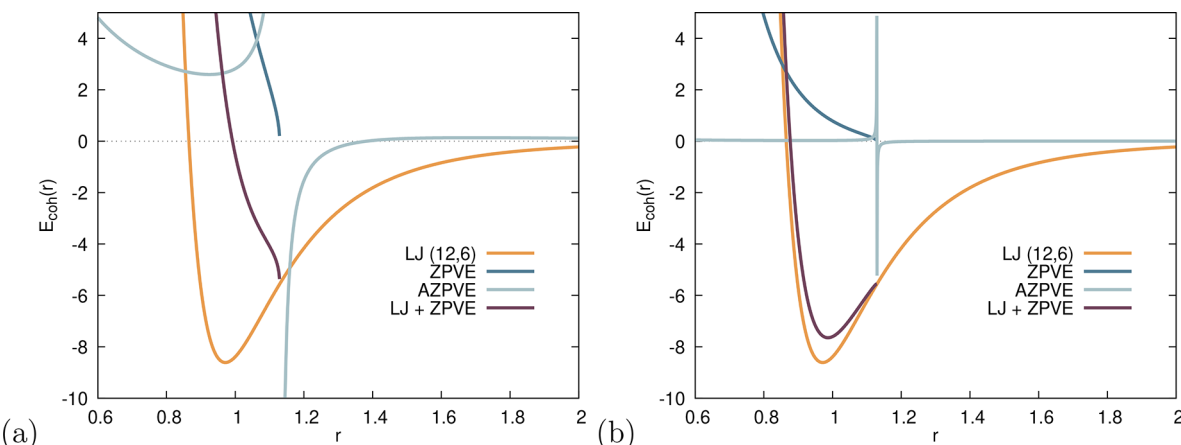


**Figure 5.** Static and dynamic contributions (only the real part of the ZPVE is shown, the expression for the ZPVE becomes complex beyond the critical distance) to the total cohesive energy for the (12, 6) LJ potential ( $\epsilon$  and  $r_e$  set to unity), for the three different masses (a)  $M = 10$  and (b)  $M = 1000$  according to eq 48.

other atoms in one dimension, as shown in parts a and b of Figure 4, results in the equality  $r_0^{\text{crit}} = r_0^{\text{infl}}$ .

For the two-dimensional case the close-packed arrangement is the hexagonal lattice (one layer of the 3D fcc lattice) for which we can derive the corresponding lattice sums in terms of Riemann  $\zeta(x)$  and Hurwitz  $h(x, y)$  functions<sup>79</sup> according to Zucker and Robertson,<sup>80</sup>

$$L_n^{2D} = 3^{1-n/2} 2\zeta\left(\frac{n}{2}\right) \left[ h\left(\frac{n}{2}, \frac{1}{3}\right) - h\left(\frac{n}{2}, \frac{2}{3}\right) \right] \quad (47)$$

There are six nearest neighbors and therefore  $L_\infty^{1D} = 6$ . We get  $L_6^{2D} = 6.37705$ ,  $L_{12}^{2D} = 6.01079$ ,  $L_8^{2D} = 6.10578$ , and  $L_{14}^{2D} = 6.00382$ . This leads to  $r_0^{2D, \text{infl}} = 1.0978r_e$  and  $r_0^{2D, \text{crit}} = 1.13724r_e$ .

For the fourth, and final, critical point let us discuss the minimal mass needed to stabilize the solid. Let us start with the minimal mass needed to form a bond between two atoms. Within the Born–Oppenheimer approximation two atoms can form a chemical bond if the ZPVE is smaller than the binding energy,  $E_{\text{ZPVE}} < \epsilon$ . This implies that, within the harmonic approximation for the ground state vibrational energy level, we need

$$E_{\text{ZPVE}} = \frac{6}{r_e} \sqrt{\frac{\epsilon}{M}} < \epsilon \quad (48)$$

from which we deduct the critical mass,

$$M_{\text{crit}}^{\text{dimer}} = \frac{36}{\epsilon r_e^2} \quad (49)$$

In this simple picture,  $M > M_{\text{crit}}^{\text{dimer}}$  is thus required to stabilize a diatomic molecule  $E_2$ . This is intuitive, as a small binding energy requires a larger critical mass to stabilize a diatomic molecule within the Born–Oppenheimer approximation. Using the values for helium in Table 2, we obtain a critical mass of  $M_{\text{crit}}^{\text{dimer}} = 17.9$  amu, which is far too high for any stable helium isotope. The harmonic ground state vibrational level lies above the diatomic  $\text{He}_2$  potential curve,<sup>81,82</sup> and only anharmonicity corrections, which are very large for this system due to the low mass and binding energy, together with an accurate treatment of the diatomic potential energy curve, can stabilize  $\text{He}_2$  to such an extend that it can be observed at ultralow temperatures.<sup>83–86</sup> Yet, the remaining dissociation energy is very small for  $\text{He}_2$ , measured to be  $5.58 \pm 0.49$  nHa compared to the (uncorrected)

binding energy shown in Table 2. In contrast, for Ne, we obtain 4.3 amu, far below the mass of the most stable isotope of  $^{20}\text{Ne}$ .

The same analysis may now be performed for the solid state, that is, we stabilize the solid described by a LJ potential if  $E_{\text{LJ}}^{\text{ZPVE}} < -E_{\text{LJ}}$  (remembering that  $E_{\text{LJ}}(r_0)$  was chosen to be negative in the attractive region). Within the Einstein approximation we obtain the following relation from the combination of eqs 4, 15, and 41,

$$M_{\text{crit}} = \frac{36}{\epsilon r_e^2} f_{\text{solid}} \quad \text{with } f_{\text{solid}} = \frac{1}{L_6^3} \left( \frac{L_6}{L_{12}} \right)^{1/3} (11L_{14}L_6 - 5L_8L_{12}) \quad (50)$$

This is identical with the result for the diatomic molecule except for the factor  $f_{\text{solid}}$ . Using the lattice sums from ref 40, we get for the different structures  $f_{\text{bcc}} = 0.4298$ ,  $f_{\text{fcc}} = 0.4005$ , and  $f_{\text{hcp}} = 0.4004$ . This reduces the helium critical mass to 7.17 amu for the fcc lattice compared to 17.9 amu for the diatomic. However, the atomic critical mass is still too large for solid helium; i.e., the  $^8\text{He}$  isotope has a half-life of 119 ms. Additionally, anharmonicity effects destabilize the rare gas solid. Phonon dispersion<sup>87</sup> most likely reduces the destabilizing harmonic ZPVE compared to the Einstein approximation,<sup>34</sup> and quantum effects beyond the Born–Oppenheimer approximation also become important for the treatment of solid helium.<sup>88</sup>

Parts a and b of Figure 5 show the cohesive energy of the (12, 6) LJ potential with  $M$  below and with mass  $M$  above the critical mass, respectively. If the mass  $M$  is small, as it is for  $^3\text{He}$  or  $^4\text{He}$ , the vibrating periodic lattice does not have a minimum; see Figure 5a where the potential curve for  $E_{\text{LJ}}(r) + E_{\text{LJ}}^{\text{ZPVE}}(r)$  abruptly ends when  $\omega_E$  becomes imaginary. Hence, the  $r_0^{\text{ZPVE}}$  values for helium are set in parentheses as this is the point when the lattice optimization stops because of  $\omega_E = 0$ . Here the perturbative treatment for anharmonicity effects completely breaks down. At larger masses the minimum is retained, see Figure 5b.

Experimentally, it is known that under pressures of approximately 2.5 MPa helium is quite unusual as it solidifies to the hcp phase,<sup>89,90</sup> and a hcp  $\rightarrow$  fcc phase transition occurs at 1.1 GPa and 15K.<sup>91</sup> Helium under extreme conditions plays an important role within the science of planets and stars.<sup>90,92–94</sup> We

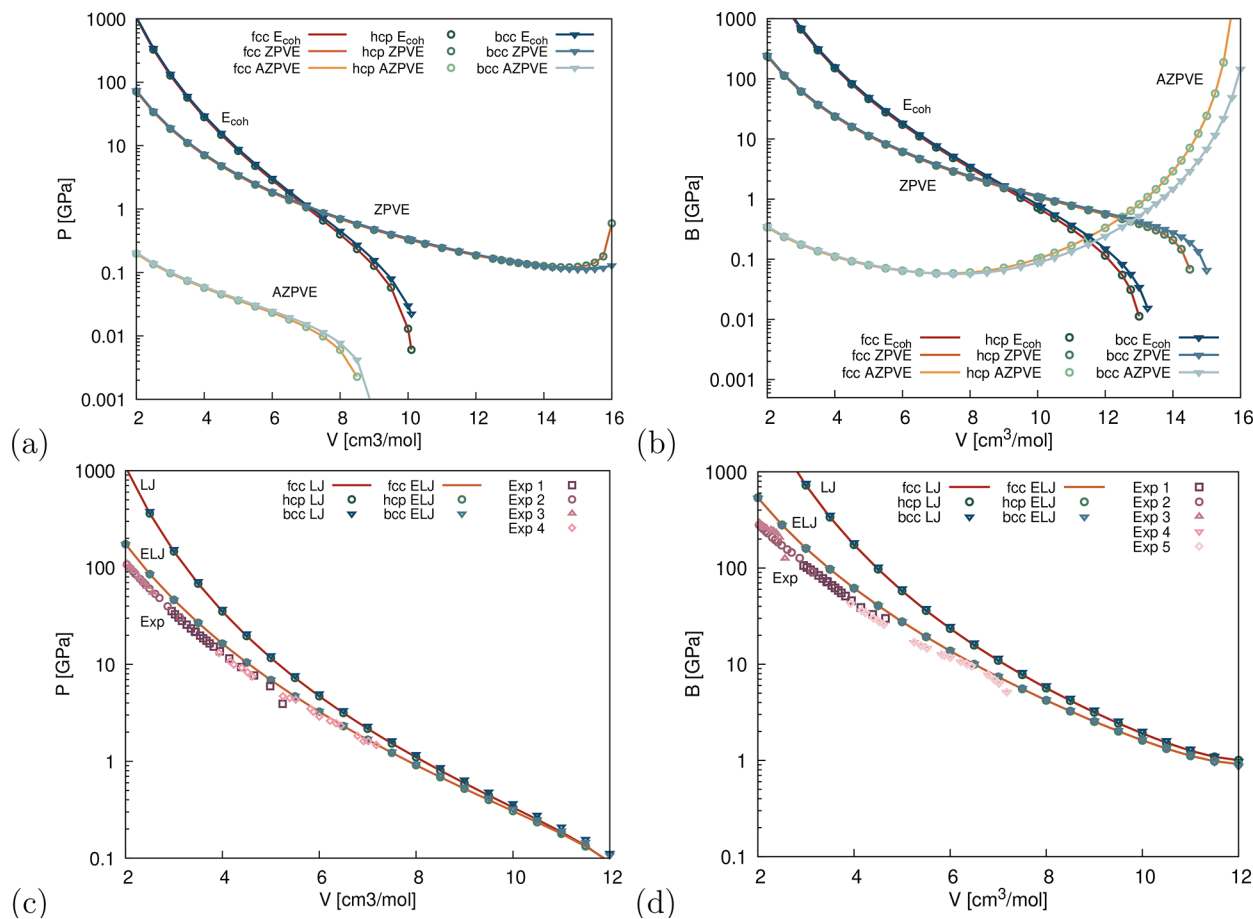


**Figure 6.** Pressure  $P(V)$  and bulk modulus  $B(V)$  curves for the fcc, hcp, and bcc phases of solid helium derived from the analytical formulas presented in this paper (logarithmic scale is used for  $P$  and  $B$ ). (a) (12–6) LJ  $P(V)$ -diagram for the different pressure contributions to the static cohesive energies  $P_{LJ}$ , harmonic zero-point vibrational  $P_{LJ}^{ZPVE}$  and anharmonic contributions  $P_{LJ}^{AZPVE}$  within the Einstein approximation. (b) Same as part a but for the bulk modulus  $B(V)$ . (c) Total pressure  $P = P_{ELJ}^{stat} + P_{ELJ}^{ZPVE} + P_{ELJ}^{AZPVE}$  for the LJ and ELJ potentials in comparison to experimental data taken from Dewaele<sup>163</sup> and from refs 105 and 106. Exp1:  $T = 15$  K, pressure gauge (PG)  $\text{SrB}_4\text{O}_7\text{Sm}^{2+}$ . Exp2:  $T = 297$  K, PG W. Exp3:  $T = 297$  K, PG ruby. Exp4:  $T = 300$  K, PG ruby. (d) Exp1–Exp3 as in part c for the bulk modulus  $B(V)$ . Exp5: extrapolated to  $T = 0$  K, isochor cell, from ref 107. For the conversion of pressure units we used 1 au =  $2.94210157 \times 10^4$  GPa. For hcp we took the ideal  $c/a = \sqrt{8/3}$  ratio, as lattice distortions are small even at higher pressures.<sup>108</sup>

therefore discuss the validity of the (12, 6) LJ model for the less critical helium high-pressure range in the following section.

**The Equation of State for Solid Helium.** Parts a–d of Figure 6 show LJ  $P(V)$  and  $B(V)$  curves for solid helium for the three different observed phases, fcc, hcp and bcc, of  ${}^4\text{He}$  in the pressure/volume range where this simple LJ Einstein model should work reasonably well.<sup>95–98</sup> To give a feeling for the volume range to be considered for bulk helium, the liquid state of  ${}^4\text{He}$  at normal pressure has a density of  $0.125 \text{ g/cm}^3$  corresponding to a very large volume of  $32 \text{ cm}^3/\text{mol}$ .<sup>99</sup> In contrast, solid helium has a density of  $0.214 \text{ g/cm}^3$  at  $6.7 \text{ GPa}$  corresponding to a volume of  $18.7 \text{ cm}^3/\text{mol}$  and nearest neighbor distance of  $r_0 = 3.528 \text{ \AA}$ , which is larger than both the inflection point,  $r_0^{\text{infl}}$ , and critical distance,  $r_0^{\text{crit}}$ ; see Table 2. This shows the limitation of the simple Einstein model for bulk helium.<sup>100</sup> Indeed, in this very low density range, zero-point vibrational energy effects dominate for both the pressure and the bulk modulus as can be seen from Figure 6, parts a and b.

Solid helium shows giant plasticity and superfluid-like mass transport at large volumes and low temperatures<sup>101,102</sup> (for a recent review, see Beamish and Balibar<sup>103</sup>), and our “static” model used here cannot accurately describe such phenomena.

Moreover, at these large volumes perturbation theory used for the anharmonicity effects breaks down and one requires a full dynamic treatment, for example by using quantum Monte Carlo simulations.<sup>88,90,104</sup> This can already be seen for the bulk moduli at volumes  $V > 12 \text{ cm}^3/\text{mol}$ , where the LJ results start to deviate substantially from the experimental results, see Figure 6d. We therefore focus on the high pressure regime instead.

Grüneisen already pointed out in 1912 that the vibrational frequency increases with pressure<sup>13</sup> because the potential energy becomes increasingly repulsive. Our Einstein model shows that harmonic vibrational contributions to the pressure dominate down to volumes of  $8 \text{ cm}^3/\text{mol}$ . Below  $8 \text{ cm}^3/\text{mol}$ , the pressure contribution coming directly from the static cohesive energy (5) starts to dominate over vibrational effects. A similar behavior is observed for the bulk modulus. Here, anharmonicity effects become even more important in the low density range. As helium represents a special case within the rare gas elements,<sup>52</sup> for the heavier rare gases, this picture changes significantly because of the increasing mass.<sup>55,63,66</sup>

We can determine the point at which the vibrational pressure becomes less important than the pressure created by the repulsive wall of the potential energy curve for a LJ potential,

that is  $P_{\text{LJ}}^{\text{ZPVE}}(V) = P_{\text{LJ}}(V)$  at a specific volume, which we denote as  $V_{\text{H}}$ . For a (12, 6) LJ potential we get a simple relation from [eqs 5](#) and [26](#),

$$f(V_{\text{H}}/V_e) = \epsilon r_e^2 M \quad (51)$$

where  $f(x)$  is an algebraic function containing only the lattice sums for a specific lattice,

$$f(x) = \left( \frac{L_6}{L_{12}} \right)^{1/3} \frac{x^4 (77L_{14} - 20L_8 x^2)^2}{4(L_{12} - L_6 x^2)^2 (11L_{14} - 5L_8 x^2)} \quad (52)$$

The left- and right-hand side of [eq 51](#) are dimensionless (either use atomic units for calculating  $\epsilon r_e^2 M$  or divide this expression by  $\hbar^2$ ). As the pressure from the cohesive energy is zero at the minimum distance, the validity range is  $x = V_{\text{H}}/V_e \ll 1$ . In any case, from the data in [Table 2](#) we get  $\epsilon r_e^2 M = 8.048$  for  ${}^4\text{He}$  and  $\epsilon r_e^2 M = 6.065$  for  ${}^3\text{He}$  corresponding to a volume ratio of  $V_{\text{H}}/V_e = 0.647$  and  $V_{\text{H}}/V_e = 0.624$  for the fcc lattice respectively (for comparison for  ${}^{20}\text{Ne}$ , we have  $V_{\text{H}}/V_e = 0.829$  and for  ${}^{40}\text{Ar}$  0.886, much closer to the minimum value  $V = V_{\text{min}}/V_e = (r_0^{\text{min}}/r_e)^3 = 0.916$ ). This demonstrates the importance of vibrational effects for  ${}^4\text{He}$  and  ${}^3\text{He}$  in the low to medium pressure range because of their low mass.

The question now arises how well this (12, 6) LJ model works. As already mentioned, in the low density range one requires a more complete quantum picture not considered here.<sup>[87,88,90,109](#)</sup>

In the high density range we can compare to experimental data from Dewaele,<sup>[163](#)</sup> as shown in [Figure 6](#), parts c and d (when bulk experimental moduli were not available, a polynomial fit to the observed  $P(V)$  data was used to obtain  $B(V)$ ). The data show that the LJ  $P(V)$  curve (containing all terms within the Einstein approximation) deviates substantially from the experimentally obtained values, and increasingly so with decreasing volume. These large deviations in the high pressure range are mostly due to the incorrect repulsive form of the (12, 6) LJ potential as has been pointed out before.<sup>[110,111](#)</sup> Of course, one can always modify the repulsive term in the LJ potential.<sup>[112,113](#)</sup>

More accurate two-body potentials  $V^{(2)}(r)$  are known for all the rare gases up to oganesson,<sup>[22,53,57–59,114–116](#)</sup> and there are already a number of theoretical studies for the  $P(V)$  curves of solid helium.<sup>[117,118](#)</sup> To further investigate the failure of the LJ potential in the high pressure range we fitted a recently published potential energy curve  $V_{\text{PCJS}}^{(2)}$  by Przybytek, Cencek, Jeziorski, and Szalewicz (PCJS) for the helium dimer,<sup>[116](#)</sup> who included adiabatic and relativistic as well as QED effects in their coupled-cluster treatment, to an ELJ potential. We used a least-squares fit procedure introducing distance dependent weights  $\omega(r)$  to take care of the very small and large energy values in the long- and short-range of the potential energy curve, respectively,

$$\frac{\partial}{\partial c_m} \int_{r_c}^{\infty} dr \omega(r) \left[ \sum_{n=1}^N c_n r^{-s_n} - V_{\text{PCJS}}^{(2)}(r) \right]^2 = 0 \quad (53)$$

which leads to a set of  $N$  linear equations for the coefficients  $c_n$  ( $m = 1, \dots, N$ ),

$$\sum_{n=1}^N c_n \int_{r_c}^{\infty} dr \omega(r) r^{-(s_n + s_m)} = \int_{r_c}^{\infty} dr \omega(r) r^{-s_m} V_{\text{PCJS}}^{(2)}(r) \quad (54)$$

We applied a numerical integration scheme, a weighting function of  $\omega(r) = 1 - e^{-ar}$  with  $a = 0.89$ , and set  $r_c$  to the lowest possible value of 2.1 au to obtain a good fit over the whole

distance range. The resulting ELJ potential yields an equilibrium distance of  $r_e = 5.6080$  au, an inflection point  $r^{\text{infl}}$  at 6.2183 au, and a binding energy of  $\epsilon = -348.746 \mu\text{Ha}$  compared to the PCJS potential of 5.6080 au, 6.2089 au, and  $-348.236 \mu\text{Ha}$ , respectively. This should give accurate two-body pressures up to about 1 TPa. We fixed the parameter  $c_1 = -C_6$  and  $c_2 = -C_8$  to the van der Waals coefficients given in [ref 116](#) to correctly describe the long-range, and we chose  $c_N > 0$  to correctly describe the repulsive short-range. The obtained parameters  $c_n$  are listed in [Table 3](#).

**Table 3. Potential Parameters for the He Dimer Obtained from a Least-Squares Fit to the Analytical Form of Szalewicz and Co-workers<sup>[116](#)</sup> (All Potential Parameters Given in Atomic Units)**

$n$	$s_n$	$c_n$	$n$	$s_n$	$c_n$
1	6	-1.4618550565137	2	8	-14.1208183897247
3	9	13997.975339736	4	10	-304327.625470953
5	11	2441586.03190761	6	12	-8163337.07262287
7	13	3390456.21241699	7	14	51324186.4628455
9	15	-118039510.368528	10	16	-31496186.3299036
11	17	456234485.18761	12	18	-639488529.764361
13	19	296722948.860609			

[Figure 7](#) shows the deviations  $[V_{\text{ELJ}}^{(2)}(r) - V_{\text{PCJS}}^{(2)}(r)]^{(n)}$  up to the second derivatives ( $n = 2$ ). As can be seen, the error in the energy

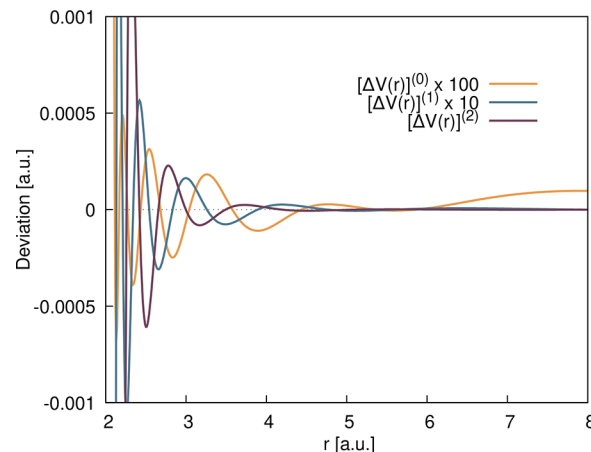


**Figure 7.** Deviations between the ELJ and the PCJS potential,  $[V_{\text{ELJ}}^{(2)}(r) - V_{\text{PCJS}}^{(2)}(r)]^{(n)}$ , up to second order in the derivatives ( $n \leq 2$ ).

is of the order of a few  $\mu\text{Ha}$  which is acceptable and the error in the first and second derivatives increase by an order of magnitude each. A test calculation with our program SAMBA<sup>[49](#)</sup> ensured that in the distance range  $r > 2.1$  au ( $V > 0.6 \text{ cm}^3/\text{mol}$  for the fcc structure) the energy, pressure and bulk moduli are in very good agreement with the results from the PCJS potential. For example, the two-body cohesive energy, pressure and bulk modulus at a small volume of  $V = 1 \text{ cm}^3/\text{mol}$  for the ELJ and PCJS potential (the latter obtained numerically and given in parentheses) are  $P = 1.2187$  (1.2183) TPa and  $B = 3.221$  (3.227) TPa.

To compare with experimental  $P(V, T)$  and  $B(V, T)$  data, one has to include the increase in pressure and bulk modulus due to finite temperature effects. For this we use the Einstein approximation ([38](#)) to obtain the thermal phonon pressure ( $\beta = 1/k_B T$ ),

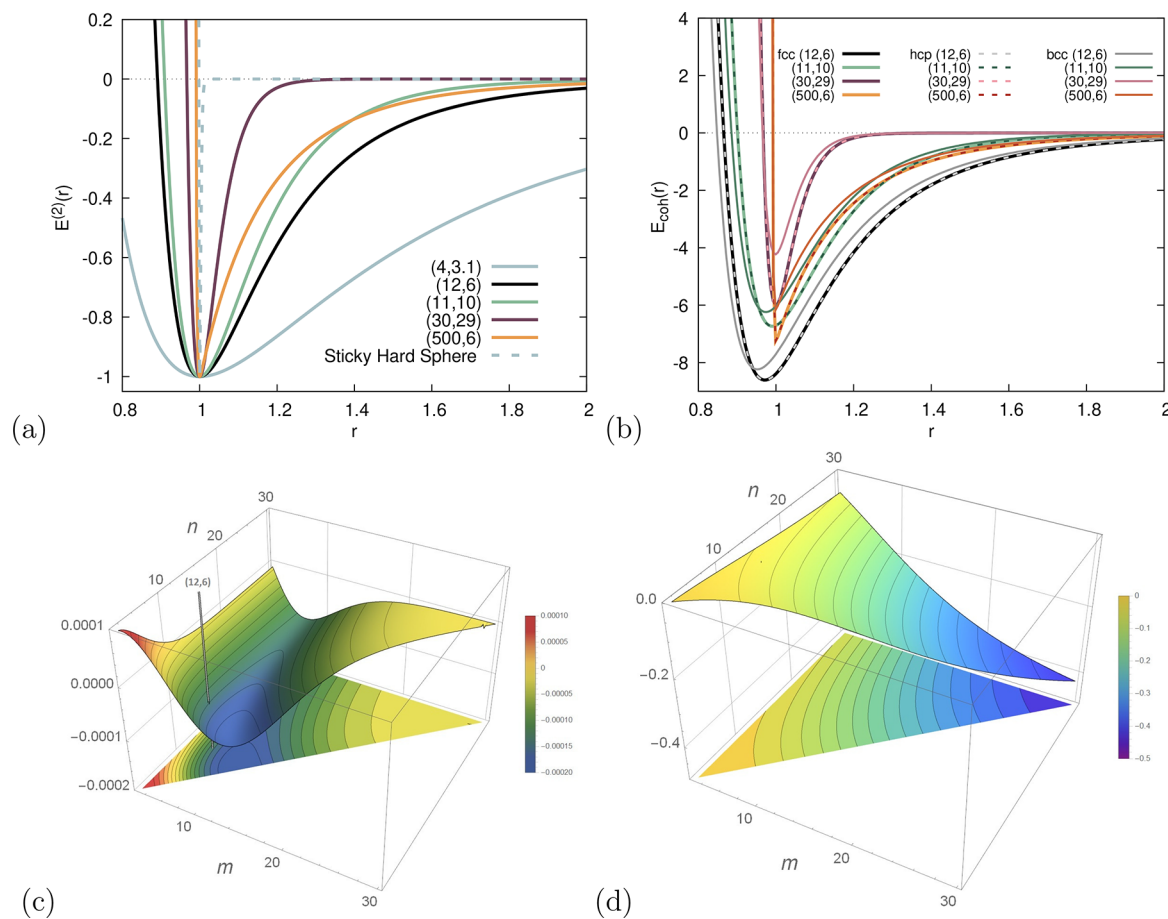


**Figure 8.** (a) Interaction potential and (b) the cohesive energy for a range of  $n$  and  $m$  values of the  $(n, m)$  LJ potentials. Relative difference in cohesive energies (c)  $\Delta_{hcp}^{fcc}(n, m)$  between the fcc and hcp phase and (d)  $\Delta_{hcp}^{bcc}(n, m)$  between the bcc and hcp phase, for different choices of  $(n, m) \in \mathbb{R}_+^2$ ,  $n > m > 3$  of the LJ potential.

$$\begin{aligned} P_{th}(V, T) &= -3 \frac{\partial \omega_E(V)}{\partial V} [e^{\beta \omega_E(V)} - 1]^{-1} \\ &= 2P_{ZPVE} [e^{\beta \omega_E(V)} - 1]^{-1} \end{aligned} \quad (55)$$

and similar for the bulk modulus,

$$\begin{aligned} B_{th}(V, T) &= B_{th1}(V, T) + B_{th2}(V, T) \\ &= 2B_{ZPVE}(V) [e^{\beta \omega_E(V)} - 1]^{-1} \\ &\quad - \frac{4}{3} P_{ZPVE}^2(V) \beta V e^{\beta \omega_E(V)} [e^{\beta \omega_E(V)} - 1]^{-2}. \end{aligned} \quad (56)$$

For an LJ or ELJ potential, we have analytical expressions for both terms through [eqs 16, 26, and 28](#). These equations show that  $P_{th} \propto P_{ZPVE}$ ,  $T$ ,  $\omega_e^{-1}$  and  $B_{th} \propto B_{ZPVE}$ ,  $T$ ,  $P_{ZPVE}^2$ ,  $\omega_e^{-1}$ . Different formulas for thermal contributions are available from the Debye model, which requires the Debye frequency and the Grüneisen parameter.<sup>119</sup> Using our two formulas, we obtain for the ELJ potential at  $T = 297$  K and  $V = 2 \text{ cm}^3/\text{mol}$  a thermal pressure component of  $P_{th} = 0.21 \text{ GPa}$  and bulk modulus of  $B_{th} = -0.69 \text{ GPa}$  ( $B_{th1} = 0.36 \text{ GPa}$ , and  $B_{th2} = -1.05 \text{ GPa}$ ). These are relatively small compared to the measured values of about  $P = 110 \text{ GPa}$  and  $B = 290 \text{ GPa}$  at that volume. We find that the  $B_{th2}$  term in [eq 56](#) dominates, leading to a negative thermal contribution to the bulk modulus, in agreement with the values provided by Zha, Mao, and Hemley.<sup>119</sup> These authors also noted relatively small values for the thermal pressure. The reason for this lies in the small  ${}^4\text{He}$  mass, resulting in a large Einstein

frequency  $\omega_E$  and small thermal contribution. It explains why the experimental temperature differences for the pressure and bulk modulus between 15 and 297 K are barely visible in [Figure 6](#), parts c and d. As shown for neon, the thermal contributions become far more important in the low-pressure regime.<sup>55</sup> We therefore neglect temperature effects for  ${}^4\text{He}$  in our discussion because the neglect of higher-body terms contains much larger errors compared to the thermal contributions.

While the qualitative LJ picture shown in [Figure 6](#), parts a and b, remains the same for the ELJ potential, the pressure and bulk moduli are a fraction smaller and much closer to the experimental values, that is because the ELJ potential describes the repulsive wall correctly in contrast to the (12, 6) LJ potential. Further improvement requires the inclusion of phonon dispersion and, more importantly, higher  $N$ -body terms in the interaction potential<sup>94,111</sup> which become attractive in the short-range.<sup>88,90,109,114,120–123</sup> For higher  $n$ -body forces analytical formulas in terms of lattice sums are unfortunately not available. Moreover, the most accurate three-body potential obtained from ab-initio data by Cencek, Patkowski, and Szalewicz (CPS)<sup>124</sup> is only valid for internuclear distances of  $r > 3.5 \text{ au}$  ( $V > 2.8 \text{ cm}^3/\text{mol}$  for the fcc structure), and to add to this, the different three-body potentials available<sup>120,124–126</sup> lead to quite different results in the short-range. Nevertheless, in the valid volume range we calculate a total pressure including three-body effects with the ELJ two-body and CPS three-body potential of 27.3 GPa at  $V = 2.954 \text{ cm}^3/\text{mol}$  compared to the experimental

value of 35.5 GPa. This underestimation of the pressure at small volumes was also noted by Chang and Boninsegni.<sup>127</sup> Bulk moduli calculations by Barnes and Hinde show that three-body interactions become very important in the short-range.<sup>122</sup> How important the three-body, and higher order, contributions are to the vibrational pressure are topics to be further investigated.

**The Difference in Lennard-Jones Cohesive Energies between the bcc, fcc, and hcp Phases.** The almost energetically degenerate fcc and hcp phases for the rare gases have been a matter of long-standing debate.<sup>29,128–132</sup> We therefore discuss the difference in cohesive energies between the different phases for a  $(n, m)$  LJ potential in more detail.

Using eqs 4 and 41, we obtain for the cohesive energy at the minimum nearest neighbor distance,

$$E_{\text{LJ}}(r_0^{\min}) = \frac{\epsilon}{2(n-m)} \left[ mL_n \left( \frac{L_m}{L_n} \right)^{n/(n-m)} - nL_m \left( \frac{L_m}{L_n} \right)^{m/(n-m)} \right], \quad m < n \quad (57)$$

Similar to the minimum neighbor distance which is directly related to the equilibrium distance of the dimer, (see eq 41), the cohesive energy is only dependent on the binding energy  $\epsilon$  of the diatomic and the ratios between LJ coefficients. From this we derive the relative difference in cohesive energies  $\Delta_{\text{P1},\text{P2}}$  between the two phases P1 and P2,

$$\begin{aligned} \Delta_{\text{P1},\text{P2}}(n, m) &= 1 - \frac{E_{\text{LJ}}^{\text{P2}}(r_0^{\text{P2}})}{E_{\text{LJ}}^{\text{P1}}(r_0^{\text{P1}})} \\ &= 1 - \frac{mL_n^{\text{P2}} \left( \frac{L_m^{\text{P2}}}{L_n^{\text{P2}}} \right)^{n/(n-m)} - nL_m^{\text{P2}} \left( \frac{L_m^{\text{P2}}}{L_n^{\text{P2}}} \right)^{m/(n-m)}}{mL_n^{\text{P1}} \left( \frac{L_m^{\text{P1}}}{L_n^{\text{P1}}} \right)^{n/(n-m)} - nL_m^{\text{P1}} \left( \frac{L_m^{\text{P1}}}{L_n^{\text{P1}}} \right)^{m/(n-m)}} \end{aligned} \quad (58)$$

For the  $(12, 6)$  LJ potential this simplifies to

$$\Delta_{\text{P1},\text{P2}}(12, 6) = 1 - \frac{L_{12}^{\text{P1}} (L_6^{\text{P2}})^2}{L_{12}^{\text{P2}} (L_6^{\text{P1}})^2} \quad (59)$$

and we obtain  $\Delta_{\text{fcc}/\text{hcp}}(12, 6) = -1.00994 \times 10^{-4}$  and  $\Delta_{\text{bcc}/\text{hcp}}(12, 6) = -4.53763 \times 10^{-2}$  using the lattice sums from ref 40. We see that such a potential prefers the hcp structure as correctly analyzed by Kihara and Koba,<sup>128</sup> although fcc is very close in energy.<sup>34,111,133</sup> For a general  $(n, m)$  LJ potential allowing for real exponents, one has to introduce unphysical soft potentials of low  $(n, m)$  values with  $n < 5.7$  to stabilize the fcc structure through two-body forces alone as parts a–d of Figure 8 show. The figures also show that hcp is preferred over bcc through the range of  $(n, m)$  values.

The preference for hcp over fcc can easily be explained. Looking at shells of atoms around one arbitrarily chosen central atom, we find the same numbers of atoms in the first and second shell for the fcc and hcp lattice. Differences only start from the third shell onward, hcp has two extra atoms at a distance of  $(n, m) \in \mathbb{R}_+^2, n > m > 3$  that are not present in the fcc structure. Therefore, at a distance of  $\sqrt{8/3} r_0$ , the fcc cluster contains 18 atoms while the hcp has already 20 atoms. The third fcc shell is found at a much larger distance of  $\sqrt{8/3} r_0$  with an additional 24 atoms.<sup>131,134</sup> This is reflected in the lattice sums, as we obtain the inequality

$$\Delta L_n^{\text{fcc}/\text{hcp}} = L_n^{\text{fcc}} - L_n^{\text{hcp}} < 0 \quad (60)$$

over whole range of real values of  $n \in \mathbb{R}_+, n \geq 3$  (also allowing for the singularity at  $n = 3$ ).<sup>40</sup> In fact,  $\Delta L_n^{\text{fcc}/\text{hcp}}$  has a minimum at  $n = 6.2448$  with  $\Delta L_n^{\text{fcc}/\text{hcp}} = -0.00097845$ , with maximum preference for the hcp structure, which is close to the dispersive  $n = 6$  term. As the  $r^{-6}$  term is the dominant interaction for the first few nearest neighboring shells, this situation does not change if we adopt a more accurate two-body potential.<sup>34</sup> This explains that for a simple LJ potential, without inclusion of zero-point vibrational effects, hcp is preferred over the fcc lattice contrary to what is known from experiment.<sup>19</sup> The only exception we find for ultrasoft LJ potentials with small  $(n, m)$  values close to the singularity of the lattice sum at  $n = 3$ . Here counting shells further away becomes important.

A special case of the  $(n, m)$  LJ potential is the Sticky Hard Sphere (SHS) potential

$$V_{\text{SHS}}(r) = \begin{cases} \infty, & r < r_e \\ -\epsilon, & r = r_e \\ 0, & r > r_e \end{cases} \quad (61)$$

which is reached in the limit  $n \rightarrow \infty, m \rightarrow \infty, n > m$ , depicted with the blue dashed line in Figure 8a. The SHS potential does not distinguish between the fcc or hcp phases; i.e., they are energetically degenerate, since both phases have, within this limit, the same packing density, representing the densest possible packings of spheres. In fact, combinations of fcc and hcp layers, the so-called Barlow packings, also belong to the most dense sphere packings.<sup>48</sup> However, such packings have not been observed experimentally, which remains an unresolved problem in the theory of lattice packings.<sup>135</sup> A SHS potential with long-range dispersion can be constructed by using the  $(n, 6)$  LJ potential with a very large  $n$  value, depicted with the orange line in Figure 8, parts a and b.<sup>136,137</sup> In this case, the cohesive energy is given by<sup>137</sup>

$$\lim_{n \rightarrow \infty} E_{\text{LJ}}(r_0) = -\epsilon \frac{L_m}{2} \left( \frac{r_e}{r_0} \right)^m \quad (62)$$

**The Difference between the fcc and hcp Phases for Solid Argon under Pressure.** In the previous section, the difference in cohesive energy between the fcc, hcp, and bcc at 0 K was discussed. To compare these phases under pressure, the enthalpy has to be considered instead. The difference in enthalpies between hcp and fcc at constant pressure  $P$  at 0 K is

$$\begin{aligned} \Delta H_{\text{hcp}/\text{fcc}}(P) &= \Delta E_{\text{hcp}/\text{fcc}}(P) + P \Delta V_{\text{hcp}/\text{fcc}}(P) \\ &= E_{\text{hcp}}[V_{\text{hcp}}(P)] - E_{\text{fcc}}[V_{\text{fcc}}(P)] + P[V_{\text{hcp}}(P) - V_{\text{fcc}}(P)] \end{aligned} \quad (63)$$

which will be used to determine if the hcp phase persists into the high pressure region for a LJ potential. Here  $E = E^{\text{coh}} + E^{\text{ZPVE}} + E^{\text{AZPVE}}$ . For a  $(12, 6)$  LJ, the potential relation between pressure and volume is given by eq 5 and

$$\begin{aligned} P(V) &= 2\epsilon r_e^6 (r_e^6 V^{-5} - 2L_6 V^{-3}) + P^{\text{ZPVE}}(V) \\ &\quad + P^{\text{AZPVE}}(V) \end{aligned} \quad (64)$$

Even if we neglect vibrational effects, for converting the pressure into volume one has to solve a fifth-order polynomial equation,  $ax^5 + bx^3 + c = 0$ , which according to the Abel–Ruffini theorem has no general analytical solution. If we add vibrational effects, both equations become more demanding, and we have to get the volume from the pressure through more complicated algebraic

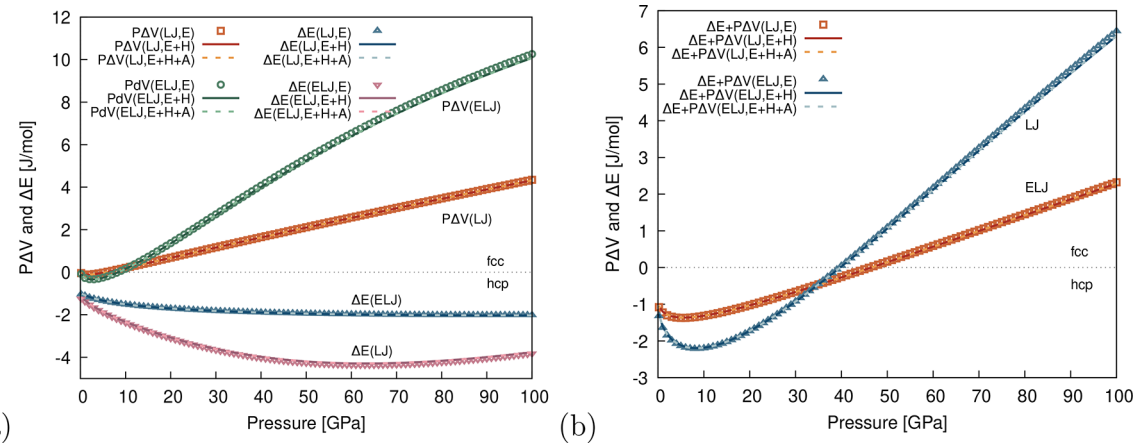


**Figure 9.** Enthalpy difference  $\Delta H_{\text{fcc/hcp}}(P)$  between fcc and hcp against the pressure  $P$  for the LJ and the ELJ potential. Negative values implies that the hcp phase is more stable. (a) lower two curves are  $\Delta E_{\text{hcp/fcc}}(P)$  plots, upper two curves  $P\Delta V_{\text{hcp/fcc}}$  plots. (b)  $\Delta E_{\text{hcp/fcc}}(P) + P\Delta V_{\text{hcp/fcc}}$ . The individual contributions are cohesive energy expression used only (E), eqs 3 and 5, harmonic ZPVE added to the cohesive energy expression (H), eqs 3, 5, 14, and 26, and finally anharmonicity corrections added (A), eqs 3, 5, 14, 21, 26, and 27.

equations, which can only be solved by numerical methods. We therefore calculate the volume  $V$  from a given pressure  $P$  by a two-point interpolation between  $(P_1, V_1)$  and  $(P_2, V_2)$  using an exponential ansatz,

$$P(V) = Ae^{-aV} \text{ with } A = P_1 e^{\ln(P_2/P_1)V_1/(V_1-V_2)} \\ \text{and } a = \frac{\ln\left(\frac{P_2}{P_1}\right)}{V_1 - V_2} \quad (65)$$

This results in an iterative process for the volume determination,

$$V_1^{(n+1)} = V_1^{(n)} + \frac{\ln[P/P_1^{(n)}]}{\ln[P_2^{(n)}/P_1^{(n)}]} [V_2^{(n)} - V_1^{(n)}] \quad (66)$$

with  $V_2^{(n)} = f_n V_1^{(n)}$  with  $f_n = 1 \pm \epsilon$  and  $\epsilon \rightarrow 0$  for  $n \rightarrow \infty$  ( $P_1$  follows from  $V_2^{(n)}$ ). In general, choosing  $f_{n+1} = f_n/a$  ( $a = 5.0$  for example) only five iterations are required to reach computer precision for the volume  $V_1^{(n)} \rightarrow V$  at a given pressure  $P$ . This procedure works well as long as the curve behaves exponential; i.e., in the region where the pressure becomes negative, a second-order polynomial fit for  $P(V)$  is preferred. We now apply this to the fcc and hcp phase of solid argon at high pressures. The individual contributions for  $\Delta H_{\text{fcc/hcp}}(P)$  up to pressures of 100 GPa are shown in Figure 9, parts a and b.

The differences in enthalpies between the fcc and hcp phase are very small (see Figure 9a) (in the  $\text{J}/\text{mol}$  range), and this small difference persists up to very high pressures. We also see that at high pressures the  $P\Delta V_{\text{hcp/fcc}}(P)$  starts to dominate over the  $\Delta E_{\text{hcp/fcc}}(P)$  term. The almost linear behavior of the  $P\Delta V_{\text{hcp/fcc}}(P)$  comes from an almost constant value of the volume difference, e.g.  $\Delta V_{\text{hcp/fcc}}(P) \approx (1.85-1.95) \times 10^{-5} \text{ cm}^3/\text{mol}$  in the high pressure range for the LJ potential. Within this model, the hcp phase is preferred at low pressures, while the fcc phase becomes more stable at pressures between 40 and 50 GPa, Figure 9b. This is in agreement with Stillinger's analysis,<sup>138</sup> which predicts an hcp  $\rightarrow$  fcc transition for the LJ potential for Ar at a volume ratio of  $V/V^{\min} = 0.537$ . This is also the case for the more accurate ELJ potential which we used from ref 54. However, this is contrary to experimental findings where a fcc phase is observed at standard conditions,<sup>71,139</sup> and a subsequent fcc-to-hcp phase transition occurs at high pressures. In fact, Errandonea et al. observed a broad fcc-to-hcp transition in room

temperature X-ray studies extending from 49.6 GPa to an estimated 300 GPa. At the highest pressure of 114 GPa, they determined a ratio of 0.3 for the amount of hcp to fcc.<sup>140</sup>

We showed recently that the fcc phase is stabilized by phonon dispersion at 0 K.<sup>34</sup> As phonon contributions play a lesser role at increased pressures, one can speculate that three-body and higher body contributions must be responsible for the phase change to hcp at higher pressures.<sup>141</sup> From a theoretical point of view, to simulate a phase transition with such small enthalpy differences remains a major challenge. If experimental data were fitted to many-body potentials, based for example on the embedded atom model, one can obtain more accurate results.<sup>142</sup>

**The Mode Grüneisen Parameter for the Rare Gas Solids.** Grüneisen stated in 1912 that the parameter  $\gamma(V, T)$  is almost independent of volume and temperature and is expected to have the same value for elements of similar structure and interaction potential.<sup>13</sup> An estimate was given by considering nearest neighbor interactions only (see ref 143), which gives the value of  $\gamma = 3.17$  for a (12, 6) LJ potential,

$$\gamma = \frac{n + m + 1}{6} \quad (67)$$

Indeed, the value varies very little for the rare gases from about 2.5 to 2.7,<sup>144,145</sup> but deviates substantially from Grüneisen's original estimate. In the following, we only consider the volume dependent mode Grüneisen parameter; for a discussion on the temperature dependence for the solid and liquid rare gas phases, we refer the reader to refs 146–149.

The Einstein approximation within the LJ model provides a more rigorous insight into the constant value of the mode Grüneisen's parameter for the noble gases. If we substitute eq 41 into eq 33, we get for the mode Grüneisen parameter at distance  $r_0 = r_0^{\min}$ ,<sup>146</sup>

$$\gamma_E^{\text{LJ}}(r_0^{\min}) = \frac{1}{6} \frac{(n+2)(n-1)L_{n+2}L_m - (m+2)(m-1)L_{m+2}L_n}{(n-1)L_{n+2}L_m - (m-1)L_{m+2}L_n} \\ \stackrel{n=12}{=} \frac{77L_{14}L_6 - 20L_8L_{12}}{33L_{14}L_6 - 15L_8L_{12}} \quad (68)$$

Table 4. Dimensionless Mode Grüneisen Parameter  $\gamma$  for the Four Different Lattices sc, bcc, fcc, and hcp<sup>a</sup>

atom	$r_0(\text{bcc})$	$\gamma_E(\text{bcc})$	$r_0(\text{fcc})$	$\gamma_E(\text{fcc})$	$r_0(\text{hcp})$	$\gamma_E(\text{hcp})$
<i>LJ</i>						
	$\left(\frac{L_{12}}{L_6}\right)^{\frac{1}{6}} r_e$	2.991928	$\left(\frac{L_{12}}{L_6}\right)^{\frac{1}{6}} r_e$	3.014083	$\left(\frac{L_{12}}{L_6}\right)^{\frac{1}{6}} r_e$	3.014102
<i>ELJ(h)</i>						
He	2.84847	3.035488	2.91126	2.767544	2.91123	2.767651
Ne	3.09254	4.076591	3.15380	3.457913	3.15376	3.457846
Ar	3.66546	3.312865	3.74303	2.971256	3.74298	2.971366
Kr	3.87459	3.171161	3.95843	2.857477	3.95839	2.857453
Xe	4.20349	3.170670	4.29406	2.851391	4.29401	2.851350
Rn	4.25436	2.921074	4.35199	2.632502	4.35193	2.632446
Og	4.09982	2.557463	4.20118	2.332987	4.20112	2.333014
<i>ELJ(h+ah)</i>						
<sup>4</sup> He	2.84847	1.889964	2.91126	2.030678	2.91123	2.030698
<sup>20</sup> Ne	3.08478	3.068178	3.14609	2.962300	3.14605	2.962298
<sup>40</sup> Ar	3.66501	3.163060	3.74258	2.886474	3.74254	2.886454
<sup>84</sup> Kr	3.87447	3.102133	3.95831	2.817675	3.95827	2.817654
<sup>132</sup> Xe	4.20344	3.127559	4.29400	2.826453	4.29396	2.826419
<sup>222</sup> Rn	4.25434	2.901018	4.35198	2.621050	4.35192	2.621010
<sup>294</sup> Og	4.09982	2.549471	4.20118	2.328094	4.20112	2.328116

<sup>a</sup>The LJ values listed are from eq 68 (the LJ value for the simple cubic structure is 2.951916). For the harmonic (*h*) and anharmonic part (*ah*) we used eqs 32 and 34. For He, we used the optimized lattice distance  $r_0^{\text{min}}$  without vibrational effects included, as inclusion of ZPVE contributions causes symmetry breaking of the lattice.

This displays that the mode Grüneisen parameter only depends on the type of lattice through their lattice sums. The corresponding values are shown in Table 4.

The LJ  $\gamma_E$  value for the fcc lattice is considerably below the value estimated by Grüneisen, which demonstrates that the summation over the whole lattice is important. Moreover, the  $\gamma_E$  values vary only slightly between the different lattices, and the difference between fcc and hcp is minuscule. Table 4 also contains ELJ results for the rare gases for both the harmonic and anharmonic approximation at the optimized nearest neighbor distances. These values show that anharmonicity effects play a major role especially for He and Ne.

Table 5 shows the mode Grüneisen parameter for the fcc lattice at the experimentally determined nearest neighbor

Table 5. Dimensionless Mode Grüneisen Parameter  $\gamma_E$  for the fcc Lattice at the Experimental Nearest Neighbor Distances<sup>139,151–153</sup> for Ne, Ar, Kr, and Xe<sup>a</sup>

atom	$r_0^{\text{exp}}$	$\gamma_E(h)$	$\gamma_E(h + ah)$	$\gamma_E(\text{exp})$
<sup>20</sup> Ne	$3.15681 \pm 0.00006$	3.4757	2.9866	$2.51 \pm 0.03$
<sup>40</sup> Ar	$3.74779 \pm 0.00006$	2.9869	2.9011	$2.7 \pm 0.1$
<sup>84</sup> Kr	$3.99223 \pm 0.00007$	2.9592	2.9126	$2.67 \pm 0.07$
<sup>132</sup> Xe	$4.3358 \pm 0.0004$	2.9754	2.9453	$2.5 \pm 0.1$

<sup>a</sup>Experimental  $\gamma$ -values are from refs 144 and 145.

distance in comparison with experimental  $\gamma$ -values. Considering that phonon dispersion and higher body effects are neglected, our results are in reasonable agreement with experiment. Previous calculations using the Debye model are also in good agreement with experiment.<sup>148,150</sup>

Figure 10 demonstrates the behavior of  $\gamma_E$  for neon over a range of volumes. It shows that, around  $V/V_e$  the ELJ and LJ curves are close, but major deviations are observed in the high-pressure regime. Equation 33 gives for the high-pressure limit at  $\gamma_E(V/V_e = 0) = (n + 2)/6$  and the point of singularity

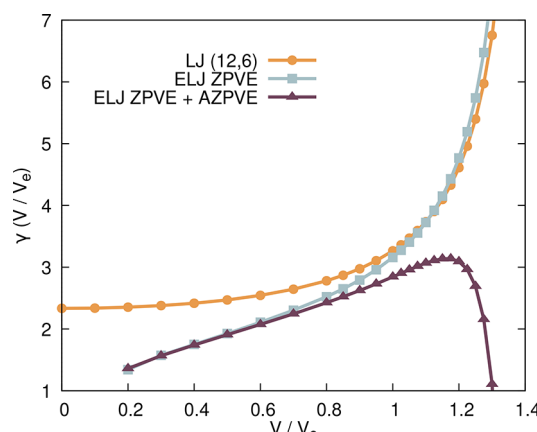


Figure 10. Grüneisen parameter  $\gamma(V/V_e)$  as a function of volume for the LJ potential and for the ELJ of Ne (harmonic and anharmonic). For  $r_e$ , we used the experimentally derived equilibrium distance of  $3.094 \pm 0.001 \text{ \AA}$ <sup>157</sup> for Ne<sub>2</sub>, resulting in a volume for solid neon of  $V_e = 12.612 \text{ cm}^3/\text{mol}$ .

$\gamma_E(V/V_e) = \infty$  happens at  $r_0^{\text{crit}}$ , eq 46, when the denominator in eq 33 becomes zero. While this behavior has been addressed before,<sup>154,155</sup> the Einstein approximation provides an analytical explanation. We observe that in the high-pressure region anharmonicity effects are small, but become important around the equilibrium distance. At distances close to  $r_0^{\text{crit}}$ , the perturbative treatment for anharmonicity effects fails. In this region, the mode Grüneisen parameter becomes very sensitive to volume changes, which will be especially important for the liquid phase (for a discussion on liquid helium, see, for example, de Souza et al.<sup>156</sup>).

## CONCLUSION

We derived analytical formulas for the vibrational contributions to the pressure and bulk modulus within the Einstein model,

which give us qualitative, yet deep insight into many bulk properties such as the mode Grüneisen parameter. The rare gases served as a good starting point to estimate harmonic and anharmonic vibrational contributions to solids. While the LJ potential may be inadequate to model interactions in solids over a large  $P(V)$  range, the ELJ potential provides analytical formulas for vibrational effects within the Einstein approximation that are capable for accurately describing two-body interactions over a large volume range.

There are many open questions in this field. It would be desirable to find approximate analytical formulas for the dynamic matrix for an ELJ potential to include phonon dispersion, as well as for the three-body potential such as the Axilrod–Teller–Muto expression<sup>72,158</sup> or similar expressions that work in the high pressure range. One could, for example, extend the work by Nijboer and deWette<sup>30,31</sup> and use the Terras expansion of quadratic forms in terms of Bessel functions.<sup>159</sup> Our group is currently trying to resolve these long-standing issues. Specifically, the fcc/hcp phases are very close in energy for the rare gases and the correct treatment of phase diagrams requires phonon dispersion and inclusion of at least three-body forces or even beyond. In particular, for helium at high pressures, such effects become crucial to correctly predict the  $P(V, T)$  and  $B(V, T)$  surfaces and phases. Moreover, for helium at low pressures, one requires a more accurate quantum treatment.<sup>88,160</sup>

## APPENDIX: DERIVATIVES OF THE EXTENDED LENNARD-JONES POTENTIAL IN THE CRYSTAL FIELD

In order to describe the vibrational motion in a lattice within the Einstein approximation ( $E$ ), we express the two-body energy of the vibrating atom at position  $\vec{r}_A$  in the ELJ field of all other (fixed) atoms  $i \in \mathbb{N}$  positioned at  $\vec{r}_i = (x_i, y_i, z_i)^T$  as

$$E(\vec{r}_A) = \sum_{i=1}^{\infty} \sum_{n>3} c_n |\vec{r}_A - \vec{r}_i|^{-n} \quad (69)$$

with,  $|\vec{r}_A - \vec{r}_i| = [(x_A - x_i)^2 + (y_A - y_i)^2 + (z_A - z_i)^2]^{1/2}$  the distance between the central vibrating atom and the other atoms  $i$ . This extends the work of Corner<sup>28</sup> and Wallace<sup>29,161,162</sup> to the terms in the ELJ potential.

A Taylor expansion in three dimensions around the minimum  $\vec{r}_A = \vec{r}_0$  of the moving atom is defined by

$$E(\vec{r}_0 + \vec{r}) = \sum_{m=0}^{\infty} \frac{1}{m!} (\vec{r} \cdot \vec{\nabla})^m E(\vec{r}_0) \quad (70)$$

This expression is understood in the sense that the derivative of  $E(\vec{r})$  has to be taken first and then evaluated at point  $\vec{r}_0$ , and  $(\vec{r} \cdot \vec{\nabla})^m$  is defined through the multinomial theorem. We conveniently put the vibrating atom at the origin,  $\vec{r}_0 = \vec{0}$ . The zero-order term just gives the cohesive energy of the crystal, and the second-order term is the expression for a harmonic oscillator in three dimensions. All derivatives in Cartesian coordinates up to fourth order with respect to the atom moving around the origin may now be derived

$$F_x = \frac{\partial E}{\partial x} \Big|_{\vec{0}} = \sum_{i,n} n c_n x_i r_i^{-n-2} \quad (71)$$

$$F_{xy} = \frac{\partial^2 E}{\partial x \partial y} \Big|_{\vec{0}} = \sum_{i,n} n(n+2) c_n x_i y_i r_i^{-n-4} \quad (72)$$

$$F_{xx} = \frac{\partial^2 E}{\partial x^2} \Big|_{\vec{0}} = \sum_{i,n} n c_n r_i^{-n-4} [(n+2)x_i^2 - r_i^2] \quad (73)$$

$$F_{xxx} = \frac{\partial^3 E}{\partial x^3} \Big|_{\vec{0}} = \sum_{i,n} n(n+2) c_n x_i r_i^{-n-6} [(n+4)x_i^2 - 3r_i^2] \quad (74)$$

$$F_{xxy} = \frac{\partial^3 E}{\partial x^2 \partial y} \Big|_{\vec{0}} = \sum_{i,n} n(n+2) c_n y_i r_i^{-n-6} [(n+4)x_i^2 - r_i^2] \quad (75)$$

$$F_{xyz} = \frac{\partial^3 E}{\partial x \partial y \partial z} \Big|_{\vec{0}} = \sum_{i,n} n(n+2)(n+4) c_n x_i y_i z_i r_i^{-n-6} \quad (76)$$

$$F_{xxxx} = \frac{\partial^4 E}{\partial x^4} \Big|_{\vec{0}} = \sum_{i,n} n(n+2) c_n r_i^{-n-8} [3r_i^4 - 6(n+4)x_i^2 r_i^2 + (n+4)(n+6)x_i^4] \quad (77)$$

$$F_{xxyy} = \frac{\partial^4 E}{\partial x^3 \partial y} \Big|_{\vec{0}} = \sum_{i,n} n(n+2)(n+4) c_n x_i y_i r_i^{-n-8} [(n+6)x_i^2 - 3r_i^2] \quad (78)$$

$$F_{xxyy} = \frac{\partial^4 E}{\partial x^2 \partial y^2} \Big|_{\vec{0}} = \sum_{i,n} n(n+2) c_n r_i^{-n-8} [r_i^4 - (n+4)(x_i^2 + y_i^2)r_i^2 + (n+4)(n+6)x_i^2 y_i^2] \quad (79)$$

$$F_{xxyz} = \frac{\partial^4 E}{\partial x^2 \partial y \partial z} \Big|_{\vec{0}} = \sum_{i,n} n(n+2)(n+4) c_n y_i z_i r_i^{-n-8} [(n+6)x_i^2 - r_i^2] \quad (80)$$

From eq 73, we derive the Laplacian  $\Delta E$  with respect to our vibrating atom,

$$\begin{aligned} \Delta E|_{\vec{0}} &= (F_{xx} + F_{yy} + F_{zz})|_{\vec{0}} = \text{Tr}\{F\}|_{\vec{0}} \\ &= \sum_{i,n} n(n-1) c_n r_i^{-n-2} \end{aligned} \quad (81)$$

The cubic lattices sc, bcc, and fcc belong to the local  $O_h$  point group. If we rotate the orthogonal coordinate system such that  $F$  is diagonal (this normal coordinate system is identical with the orthogonal coordinate system commonly used for the cubic Bravais lattices), we have  $F_{xx} = F_{yy} = F_{zz}$  because of  $O_h$  symmetry (not for hcp as already mentioned).<sup>29</sup> Thus, we obtain

$$F_{xx}^c|_0 = \frac{1}{3} \Delta E|_0 = \frac{1}{3} \sum_{i,n} n(n-1)c_n r_i^{-n-2} \quad (82)$$

where (c) stands for one of the cubic lattices. In this case we obtain also simple relationships for the quartic force constants; and  $F_{xxxx}^c = F_{yyyy}^c = F_{zzzz}^c$ .<sup>29</sup> Furthermore, we have  $F_{xxyy}^c = F_{xyyz}^c = 0$ . Because  $O_h$  contains inversion symmetry, we also have  $F_{x^i y^j z^k}^c = 0$  for any odd combination  $(i+j+k)$ , for example  $F_x^c = 0$ ,  $F_{xxx}^c = 0$ ,  $F_{xyy}^c = 0$ , and  $F_{xyz}^c = 0$ . Thus, all odd derivatives vanish, and for these lattices, we only have to consider the quartic force constants for the anharmonicity correction (see below). Using these symmetry relations, we can further simplify the two important (nonzero) quartic force constants for the cubic lattices,

$$F_{xxxx}^c|_0 = \frac{1}{3}(F_{xxxx} + F_{yyyy} + F_{zzzz})|_0 \quad (83)$$

and

$$F_{xxyy}^c|_0 = \frac{1}{3}(F_{xxyy} + F_{xxzz} + F_{yyzz})|_0 \quad (84)$$

which gives

$$F_{xxxx}^c|_0 = \frac{1}{3} \sum_{i,n} n(n+2)c_n r_i^{-n-8}[(n+4)(n+6)(x_i^4 + y_i^4 + z_i^4) - 3(2n+5)r_i^4] \quad (85)$$

and

$$F_{xxyy}^c|_0 = \frac{1}{3} \sum_{i,n} n(n+2)c_n r_i^{-n-8}[(n+4)(n+6)(x_i^2 y_i^2 + y_i^2 z_i^2 + x_i^2 z_i^2) - (2n+5)r_i^4] \quad (86)$$

No further simplification is possible. However, we can combine eqs 85 and 86, and we obtain

$$F_{xxxx}^c|_0 + 2F_{xxyy}^c|_0 = \frac{1}{3} \sum_{i,n} (n+2)(n+1)n(n-1)c_n r_i^{-n-4} \quad (87)$$

## ■ AUTHOR INFORMATION

### Corresponding Author

**Peter Schwerdtfeger** — Centre for Theoretical Chemistry and Physics, The New Zealand Institute for Advanced Study (NZIAS), Massey University Albany, Auckland 0745, New Zealand; [orcid.org/0000-0003-4845-686X](https://orcid.org/0000-0003-4845-686X); Email: [peter.schwerdtfeger@gmail.com](mailto:peter.schwerdtfeger@gmail.com)

### Authors

**Antony Burrows** — Centre for Theoretical Chemistry and Physics, The New Zealand Institute for Advanced Study (NZIAS), Massey University Albany, Auckland 0745, New Zealand

**Odile R. Smits** — Centre for Theoretical Chemistry and Physics, The New Zealand Institute for Advanced Study (NZIAS), Massey University Albany, Auckland 0745, New Zealand

Complete contact information is available at:

<https://pubs.acs.org/10.1021/acs.jpca.1c00012>

### Notes

The authors declare no competing financial interest.

## ■ ACKNOWLEDGMENTS

This work was sponsored by the Marsden Fund administered by the New Zealand Royal Society and was part of the “Molecules in Extreme Environments” project funded by the Centre for Advanced Study at the Norwegian Academy of Science and Letters, Oslo, Norway. We thank Dr. Agnes Dewaele (CEA, DAM, DIF, Arpajon, France) for providing unpublished  $P(V)$  data for  ${}^4\text{He}$  and both Assoc. Prof. Shaun Cooper (Massey University) and Dr. Elke Pahl (Auckland University) for discussions.

## ■ REFERENCES

- (1) Jones, J. E. On the Determination of Molecular Fields. I. From the Variation of the Viscosity of a Gas with Temperature. *Proc. R. Soc. London A* **1924**, *106*, 441–462.
- (2) Jones, J. E. On the Determination of Molecular Fields. II. From the Equation of State of a Gas. *Proc. R. Soc. London A* **1924**, *106*, 463–477.
- (3) Simon, F.; von Simson, C. Die Kristallstruktur des Argons. *Z. Phys.* **1924**, *25*, 160–164.
- (4) Lennard-Jones, J. E. Cohesion. *Proc. Phys. Soc.* **1931**, *43*, 461.
- (5) Lennard-Jones, J. The equation of state of gases and critical phenomena. *Physica* **1937**, *4*, 941–956.
- (6) Morse, P. M. Diatomic Molecules According to the Wave Mechanics. II. Vibrational Levels. *Phys. Rev.* **1929**, *34*, 57–64.
- (7) Wang, J.; Wolf, R. M.; Caldwell, J. W.; Kollman, P. A.; Case, D. A. Development and testing of a general amber force field. *J. Comput. Chem.* **2004**, *25*, 1157–1174.
- (8) Gnan, N.; Schröder, T. B.; Pedersen, U. R.; Bailey, N. P.; Dyre, J. C. Pressure-energy correlations in liquids. IV. “Isomorphs” in liquid phase diagrams. *J. Chem. Phys.* **2009**, *131*, 234504.
- (9) Albrechtsen, D. E.; Olsen, A. E.; Pedersen, U. R.; Schröder, T. B.; Dyre, J. C. Isomorph invariance of the structure and dynamics of classical crystals. *Phys. Rev. B: Condens. Matter Mater. Phys.* **2014**, *90*, 094106.
- (10) Stephan, S.; Thol, M.; Vrabec, J.; Hasse, H. Thermophysical Properties of the Lennard-Jones Fluid: Database and Data Assessment. *J. Chem. Inf. Model.* **2019**, *59*, 4248–4265.
- (11) Stephan, S.; Staubach, J.; Hasse, H. Review and comparison of equations of state for the Lennard-Jones fluid. *Fluid Phase Equilib.* **2020**, *523*, 112772.
- (12) Mie, G. Zur kinetischen Theorie der einatomigen Körper. *Ann. Phys.* **1903**, *316*, 657–697.
- (13) Grüneisen, E. Theorie des festen Zustandes einatomiger Elemente. *Ann. Phys.* **1912**, *344*, 257–306.
- (14) Kratzer, A. Die ultravioletten Rotationspektren der Halogenwasserstoffe. *Eur. Phys. J. A* **1920**, *3*, 289–307.
- (15) Born, M.; Landé, A. Über die Berechnung der Kompressibilität regulärer Kristalle aus der Gittertheorie. *Verh. Deut. Phys. Ges.* **1918**, *20*, 210–211.
- (16) Madelung, E. Das elektrische Feld in Systemen von regelmäßig angeordneten Punktladungen. *Phys. Z.* **1918**, *19*, 32.
- (17) London, F. Zur Theorie und Systematik der Molekularkräfte. *Eur. Phys. J. A* **1930**, *63*, 245–279.
- (18) Born, M.; Misra, R. D. On the stability of crystal lattices. IV. *Math. Proc. Cambridge Philos. Soc.* **1940**, *36*, 466–478.
- (19) Schwerdtfeger, P.; Gaston, N.; Krawczyk, R. P.; Tonner, R.; Moyano, G. E. Extension of the Lennard-Jones potential: Theoretical investigations into rare-gas clusters and crystal lattices of He, Ne, Ar, and Kr using many-body interaction expansions. *Phys. Rev. B: Condens. Matter Mater. Phys.* **2006**, *73*, 064112.
- (20) Pahl, E.; Figgen, D.; Thierfelder, C.; Peterson, K. A.; Calvo, F.; Schwerdtfeger, P. A highly accurate potential energy curve for the mercury dimer. *J. Chem. Phys.* **2010**, *132*, 114301.
- (21) Tang, K. T.; Toennies, J. P. An improved simple model for the van der Waals potential based on universal damping functions for the dispersion coefficients. *J. Chem. Phys.* **1984**, *80*, 3726–3741.

(22) Jäger, B.; Hellmann, R.; Bich, E.; Vogel, E. *Ab initio* pair potential energy curve for the argon atom pair and thermophysical properties of the dilute argon gas. I. Argon-argon interatomic potential and rovibrational spectra. *Mol. Phys.* **2009**, *107*, 2181–2188.

(23) Patkowski, K.; Szalewicz, K. Argon pair potential at basis set and excitation limits. *J. Chem. Phys.* **2010**, *133*, 094304.

(24) Jones, J. E. On the Determination of Molecular Fields. III. From Crystal Measurements and Kinetic Theory Data. *Proc. R. Soc. London A* **1924**, *106*, 709–718.

(25) Jones, J. E.; Ingham, A. E. On the Calculation of Certain Crystal Potential Constants, and on the Cubic Crystal of Least Potential Energy. *Proc. R. Soc. London A* **1925**, *107*, 636–653.

(26) Borwein, J. M.; Glasser, M.; McPhedran, R.; Wan, J.; Zucker, I. *Lattice sums then and now*; Cambridge University Press: 2013.

(27) Herzfeld, K. F.; Mayer, M. G. On the Theory of Fusion. *Phys. Rev.* **1934**, *46*, 995–1001.

(28) Corner, J. Zero-point energy and lattice distances. *Trans. Faraday Soc.* **1939**, *35*, 711–716.

(29) Wallace, D. C.; Patrick, J. L. Stability of Crystal Lattices. *Phys. Rev.* **1965**, *137*, A152–A160.

(30) Nijboer, B.; De Wette, F. W. Lattice vibrations of a f.c.c. crystal with Lennard-Jones interaction for varying lattice constant. *Phys. Lett.* **1965**, *17*, 256–258.

(31) De Wette, F.; Fowler, L.; Nijboer, B. Lattice dynamics, thermal expansion and specific heat of a Lennard-Jones solid in the quasi-harmonic approximation. *Physica* **1971**, *54*, 292–304.

(32) Einstein, A. Die Plancksche Theorie der Strahlung und die Theorie der spezifischen Wärme. *Ann. Phys.* **1907**, *327*, 180–190.

(33) Hermann, A.; Krawczyk, R. P.; Lein, M.; Schwerdtfeger, P.; Hamilton, I. P.; Stewart, J. J. P. Convergence of the many-body expansion of interaction potentials: From van der Waals to covalent and metallic systems. *Phys. Rev. A: At., Mol., Opt. Phys.* **2007**, *76*, 013202.

(34) Schwerdtfeger, P.; Tonner, R.; Moyano, G. E.; Pahl, E. Towards J/mol Accuracy for the Cohesive Energy of Solid Argon. *Angew. Chem., Int. Ed.* **2016**, *55*, 12200–12205.

(35) Borwein, D.; Borwein, J.; Pinner, C. Convergence of Madelung-like lattice sums. *Trans. Am. Math. Soc.* **1998**, *350*, 3131–3167.

(36) Born, M.; Huang, K. *Dynamical theory of crystal lattices*; Oxford University Press: 1998.

(37) Glasser, M.; Zucker, I. Lattice sums. *Theoretical chemistry: Advances and perspectives* **1980**, *5*, 67–139.

(38) Borwein, D.; Borwein, J. M.; Taylor, K. F. Convergence of lattice sums and Madelung's constant. *J. Math. Phys.* **1985**, *26*, 2999–3009.

(39) Stein, M. A fast, parallel algorithm for distant-dependent calculation of crystal properties. *Comput. Phys. Commun.* **2017**, *221*, 273–281.

(40) Burrows, A.; Cooper, S.; Pahl, E.; Schwerdtfeger, P. Analytical methods for fast converging lattice sums for cubic and hexagonal close-packed structures. *J. Math. Phys.* **2020**, *61*, 123503.

(41) Kane, G.; Goeppert-Mayer, M. Lattice Summations for Hexagonal Close-Packed Crystals. *J. Chem. Phys.* **1940**, *8*, 642.

(42) Conway, J. H.; Sloane, N. J. A. *Sphere packings, lattices and groups*; Springer: New York, 2013; Vol. 290.

(43) Schwerdtfeger, P.; Burrows, A. Program Jones - A Fortran Program for sc, bcc, fcc and hcp Lattice Sums. 2019; <http://ctcp.massey.ac.nz/index.php?group=&page=fullerenes&menu=latticesums>.

(44) Barron, T. LXXXII. On the thermal expansion of solids at low temperatures. *London, Edinburgh, and Dublin Philosophical Magazine and Journal of Science* **1955**, *46*, 720–734.

(45) Poirier, J.-P. *Introduction to the Physics of the Earth's Interior*, 2nd ed.; Cambridge University Press: 2000.

(46) Stacey, F. D.; Hodgkinson, J. H. Thermodynamics with the Grüneisen parameter: Fundamentals and applications to high pressure physics and geophysics. *Phys. Earth Planet. Inter.* **2019**, *286*, 42–68.

(47) Anderson, O. L. The Grüneisen ratio for the last 30 years. *Geophys. J. Int.* **2000**, *143*, 279–294.

(48) Barlow, W. Probable Nature of the Internal Symmetry of Crystals. *Nature* **1883**, *29*, 205–207.

(49) Schwerdtfeger, P. *Program SAMBA - A Fortran Program for optimizing and analyzing solid state structures by the use of a many-body expansion in terms of interaction potentials*; Massey University: 2020.

(50) Anderson, D. L. *Theory of the Earth*; Blackwell Scientific Publications: 1989.

(51) Pollack, G. L. The Solid State of Rare Gases. *Rev. Mod. Phys.* **1964**, *36*, 748–791.

(52) Horton, G. *Rare Gas Solids*; Academic, New York, 1976; Vol. 1.

(53) Kalos, M. H.; Lee, M. A.; Whitlock, P. A.; Chester, G. V. Modern potentials and the properties of condensed  $^4\text{He}$ . *Phys. Rev. B: Condens. Matter Mater. Phys.* **1981**, *24*, 115–130.

(54) Pahl, E.; Calvo, F.; Koči, L.; Schwerdtfeger, P. Accurate Melting Temperatures for Neon and Argon from Ab Initio Monte Carlo Simulations. *Angew. Chem., Int. Ed.* **2008**, *47*, 8207–8210.

(55) Schwerdtfeger, P.; Hermann, A. Equation of state for solid neon from quantum theory. *Phys. Rev. B: Condens. Matter Mater. Phys.* **2009**, *80*, 064106.

(56) Wiebke, J.; Pahl, E.; Schwerdtfeger, P. Melting at High Pressure: Can First-Principles Computational Chemistry Challenge Diamond-Anvil Cell Experiments? *Angew. Chem., Int. Ed.* **2013**, *52*, 13202–13205.

(57) Cencek, W.; Przybytek, M.; Komasa, J.; Mehl, J. B.; Jeziorski, B.; Szalewicz, K. Effects of adiabatic, relativistic, and quantum electrodynamics interactions on the pair potential and thermophysical properties of helium. *J. Chem. Phys.* **2012**, *136*, 224303.

(58) Bich, E.; Hellmann, R.; Vogel, E. Erratum: *Ab initio* potential energy curve for the neon atom pair and thermophysical properties for the dilute neon gas. II. Thermophysical properties for low-density neon. *Mol. Phys.* **2008**, *106*, 1107–1122.

(59) Shee, A.; Knecht, S.; Sauer, T. A theoretical benchmark study of the spectroscopic constants of the very heavy rare gas dimers. *Phys. Chem. Chem. Phys.* **2015**, *17*, 10978–10986.

(60) Smits, O. R.; Jerabek, P.; Pahl, E.; Schwerdtfeger, P. First-principles melting of krypton and xenon based on many-body relativistic coupled-cluster interaction potentials. *Phys. Rev. B: Condens. Matter Mater. Phys.* **2020**, *101*, 104103.

(61) Smits, O. R.; Jerabek, P.; Pahl, E.; Schwerdtfeger, P. A Hundred-Year-Old Experiment Re-evaluated: Accurate Ab-Initio Monte Carlo Simulations of the Melting of Radon. *Angew. Chem., Int. Ed.* **2018**, *57*, 9961–9964.

(62) Jerabek, P.; Smits, O. R.; Mewes, J.-M.; Peterson, K. A.; Schwerdtfeger, P. Solid Oganesson via a Many-Body Interaction Expansion Based on Relativistic Coupled-Cluster Theory and from Plane-Wave Relativistic Density Functional Theory. *J. Phys. Chem. A* **2019**, *123*, 4201–4211.

(63) Rościszewski, K.; Paulus, B.; Fulde, P.; Stoll, H. *Ab initio* calculation of ground-state properties of rare-gas crystals. *Phys. Rev. B: Condens. Matter Mater. Phys.* **1999**, *60*, 7905–7910.

(64) McConville, G. T. New values of sublimation energy L0 for natural neon and its isotopes. *J. Chem. Phys.* **1974**, *60*, 4093–4093.

(65) Schwalbe, L. A.; Crawford, R. K.; Chen, H. H.; Aziz, R. A. Thermodynamic consistency of vapor pressure and calorimetric data for argon, krypton, and xenon. *J. Chem. Phys.* **1977**, *66*, 4493–4502.

(66) Rościszewski, K.; Paulus, B.; Fulde, P.; Stoll, H. *Ab initio* coupled-cluster calculations for the fcc and hcp structures of rare-gas solids. *Phys. Rev. B: Condens. Matter Mater. Phys.* **2000**, *62*, 5482–5488.

(67) Cencek, W.; Patkowski, K.; Szalewicz, K. Full-configuration-interaction calculation of three-body nonadditive contribution to helium interaction potential. *J. Chem. Phys.* **2009**, *131*, 064105.

(68) Giuliani, S. A.; Matheson, Z.; Nazarewicz, W.; Olsen, E.; Reinhard, P.-G.; Sadhukhan, J.; Schuetrumpf, B.; Schunck, N.; Schwerdtfeger, P. Colloquium: Superheavy elements: Oganesson and beyond. *Rev. Mod. Phys.* **2019**, *91*, 011001.

(69) Schwerdtfeger, P.; Smits, O. R.; Pyykkö, P. The periodic table and the physics that drives it. *Nature Rev. Chem.* **2020**, *4*, 359.

(70) Smits, O. R.; Mewes, J.-M.; Jerabek, P.; Schwerdtfeger, P. Oganesson: A Noble Gas Element That Is Neither Noble Nor a Gas. *Angew. Chem., Int. Ed.* **2020**, *59*, 23636–23640.

(71) Barrett, C. S.; Meyer, L. X-Ray Diffraction Study of Solid Argon. *J. Chem. Phys.* **1964**, *41*, 1078–1081.

(72) Axilrod, B. M.; Teller, E. Interaction of the van der Waals Type Between Three Atoms. *J. Chem. Phys.* **1943**, *11*, 299–300.

(73) Kresse, G.; Hafner, J. Ab initio simulation of the metal/nonmetal transition in expanded fluid mercury. *Phys. Rev. B: Condens. Matter Mater. Phys.* **1997**, *55*, 7539–7548.

(74) Cotterill, R. M.; Tallon, J. L. Melting and the liquid and glassy states. *Faraday Discuss. Chem. Soc.* **1980**, *69*, 241–260.

(75) Tallon, J. L. A hierarchy of catastrophes as a succession of stability limits for the crystalline state. *Nature* **1989**, *342*, 658–670.

(76) Peierls, R. E. *Quantum theory of solids*; Clarendon Press: Oxford, U.K., 1996.

(77) Kartoon, D.; Argaman, U.; Makov, G. Driving forces behind the distortion of one-dimensional monatomic chains: Peierls theorem revisited. *Phys. Rev. B: Condens. Matter Mater. Phys.* **2018**, *98*, 165429.

(78) Hooton, D. L. A new treatment of anharmonicity in lattice thermodynamics: I. *London, Edinburgh, and Dublin Philosophical Magazine and Journal of Science* **1955**, *46*, 422–432.

(79) Coffey, M. W. On some series representations of the Hurwitz zeta function. *J. Comput. Appl. Math.* **2008**, *216*, 297–305.

(80) Zucker, I. J.; Robertson, M. M. Exact values of some two-dimensional lattice sums. *J. Phys. A: Math. Gen.* **1975**, *8*, 874.

(81) Lo, J. Q. W.; Shizgal, B. D. An efficient mapped pseudospectral method for weakly bound states: vibrational states of  $\text{He}_2$ ,  $\text{Ne}_2$ ,  $\text{Ar}_2$  and  $\text{Cs}_2$ . *J. Phys. B: At., Mol. Opt. Phys.* **2008**, *41*, 185103.

(82) Cencek, W.; Przybytek, M.; Komasa, J.; Mehl, J. B.; Jeziorski, B.; Szalewicz, K. Effects of adiabatic, relativistic, and quantum electrodynamics interactions on the pair potential and thermophysical properties of helium. *J. Chem. Phys.* **2012**, *136*, 224303.

(83) Luo, F.; McBane, G. C.; Kim, G.; Giese, C. F.; Gentry, W. R. The weakest bond: Experimental observation of helium dimer. *J. Chem. Phys.* **1993**, *98*, 3564–3567.

(84) Schöllkopf, W.; Toennies, J. P. Nondestructive Mass Selection of Small van der Waals Clusters. *Science* **1994**, *266*, 1345–1348.

(85) Grisenti, R. E.; Schöllkopf, W.; Toennies, J. P.; Hegerfeldt, G. C.; Köhler, T.; Stoll, M. Determination of the Bond Length and Binding Energy of the Helium Dimer by Diffraction from a Transmission Grating. *Phys. Rev. Lett.* **2000**, *85*, 2284–2287.

(86) Zeller, S.; Kunitski, M.; Voigtsberger, J.; Kalinin, A.; Schottelius, A.; Schober, C.; Waitz, M.; Sann, H.; Hartung, A.; Bauer, T.; et al. Imaging the  $\text{He}_2$  quantum halo state using a free electron laser. *Proc. Natl. Acad. Sci. U. S. A.* **2016**, *113*, 14651–14655.

(87) Eckert, J.; Thominson, W.; Shirane, G. Lattice dynamics of fcc helium at high pressure. *Phys. Rev. B* **1977**, *16*, 1057–1067.

(88) Ceperley, D. M. Path integrals in the theory of condensed helium. *Rev. Mod. Phys.* **1995**, *67*, 279–355.

(89) Simon, F.; Swenson, C. The liquid-solid transition in helium near absolute zero. *Nature* **1950**, *165*, 829–831.

(90) McMahon, J. M.; Morales, M. A.; Pierleoni, C.; Ceperley, D. M. The properties of hydrogen and helium under extreme conditions. *Rev. Mod. Phys.* **2012**, *84*, 1607–1653.

(91) Dugdale, J. S.; Simon, F. E. Thermodynamic properties and melting of solid helium. *Proc. R. Soc. London A, Math. Phys. Sci.* **1953**, *218*, 291–310.

(92) Saumon, D.; Guillot, T. Shock Compression of Deuterium and the Interiors of Jupiter and Saturn. *Astrophys. J.* **2004**, *609*, 1170–1180.

(93) Stixrude, L.; Jeanloz, R. Fluid helium at conditions of giant planetary interiors. *Proc. Natl. Acad. Sci. U. S. A.* **2008**, *105*, 11071–11075.

(94) Khairallah, S. A.; Militzer, B. First-Principles Studies of the Metallization and the Equation of State of Solid Helium. *Phys. Rev. Lett.* **2008**, *101*, 106407.

(95) Edwards, D. O.; Pandorf, R. C. Heat Capacity and Other Properties of Hexagonal Close-Packed Helium-4. *Phys. Rev.* **1965**, *140*, A816–A825.

(96) Edwards, D. O.; Pandorf, R. C. Heat Capacity and Other Properties of Body-Centered Cubic  $\text{He}^4$ . *Phys. Rev.* **1966**, *144*, 143–151.

(97) Holian, B. L.; Gwinn, W. D.; Luntz, A. C.; Alder, B. J. Predictions of the solid helium phase diagram. *J. Chem. Phys.* **1973**, *59*, 5444–5454.

(98) Young, D. A.; McMahan, A. K.; Ross, M. Equation of state and melting curve of helium to very high pressure. *Phys. Rev. B: Condens. Matter Mater. Phys.* **1981**, *24*, 5119–5127.

(99) Lide, D. R. *CRC Handbook of Chemistry and Physics*, 86th ed.; CRC press: Boca Raton, FL, 2004; Vol. 85.

(100) Henshaw, D. G. Structure of Solid Helium by Neutron Diffraction. *Phys. Rev.* **1958**, *109*, 328–330.

(101) Hunt, B.; Pratt, E.; Gadagkar, V.; Yamashita, M.; Balatsky, A. V.; Davis, J. C. Evidence for a Superglass State in Solid  $\text{He}^4$ . *Science* **2009**, *324*, 632–636.

(102) Landinez Borda, E. J.; Cai, W.; de Koning, M. Dislocation Structure and Mobility in hcp  $\text{He}^4$ . *Phys. Rev. Lett.* **2016**, *117*, 045301.

(103) Beamish, J.; Balibar, S. Mechanical behavior of solid helium: Elasticity, plasticity, and defects. *Rev. Mod. Phys.* **2020**, *92*, 045002.

(104) Cazorla, C.; Boronat, J. First-principles modeling of three-body interactions in highly compressed solid helium. *Phys. Rev. B: Condens. Matter Mater. Phys.* **2015**, *92*, 224113.

(105) Mao, H. K.; Hemley, R. J.; Wu, Y.; Jephcoat, A. P.; Finger, L. W.; Zha, C. S.; Bassett, W. A. High-Pressure Phase Diagram and Equation of State of Solid Helium from Single-Crystal X-Ray Diffraction to 23.3 GPa. *Phys. Rev. Lett.* **1988**, *60*, 2649–2652.

(106) Loubeyre, P.; LeToullc, R.; Pinceaux, J. P.; Mao, H. K.; Hu, J.; Hemley, R. J. Equation of state and phase diagram of solid  $\text{He}^4$  from single-crystal x-ray diffraction over a large P-T domain. *Phys. Rev. Lett.* **1993**, *71*, 2272–2275.

(107) Driessen, A.; van der Poll, E.; Silvera, I. F. Equation of state of solid  $\text{He}^4$ . *Phys. Rev. B: Condens. Matter Mater. Phys.* **1986**, *33*, 3269–3288.

(108) Freiman, Y. A.; Tretyak, S. M.; Grechnev, A.; Goncharov, A. F.; Tse, J. S.; Errandonea, D.; Mao, H.-k.; Hemley, R. J. Lattice distortion of hcp solid helium under pressure. *Phys. Rev. B: Condens. Matter Mater. Phys.* **2009**, *80*, 094112.

(109) Ceperley, D. M.; Alder, B. J. Ground state of solid hydrogen at high pressures. *Phys. Rev. B: Condens. Matter Mater. Phys.* **1987**, *36*, 2092–2106.

(110) Polian, A.; Grimsditch, M. Elastic Properties and Density of Helium up to 20 GPa. *Europhys. Lett. (EPL)* **1986**, *2*, 849–855.

(111) Loubeyre, P. Three-body exchange interaction in dense helium. *Phys. Rev. Lett.* **1987**, *58*, 1857–1860.

(112) Ross, M. The repulsive forces in dense argon. *J. Chem. Phys.* **1980**, *73*, 4445–4450.

(113) Sadus, R. J. Combining intermolecular potentials for the prediction of fluid properties: Two-body and three-body interactions. *J. Chem. Phys.* **2020**, *153*, 214509.

(114) Ross, M.; Young, D. A. Helium at high density. *Phys. Lett. A* **1986**, *118*, 463–466.

(115) Aziz, R. A.; Slaman, M. J. An examination of ab initio results for the helium potential energy curve. *J. Chem. Phys.* **1991**, *94*, 8047–8053.

(116) Przybytek, M.; Cencek, W.; Jeziorski, B.; Szalewicz, K. Pair Potential with Submillikelvin Uncertainties and Nonadiabatic Treatment of the Halo State of the Helium Dimer. *Phys. Rev. Lett.* **2017**, *119*, 123401.

(117) Moroni, S.; Pederiva, F.; Fantoni, S.; Boninseggi, M. Equation of State of Solid  $\text{He}^3$ . *Phys. Rev. Lett.* **2000**, *84*, 2650–2653.

(118) Herrero, C. P. Solid helium at high pressure: a path-integral Monte Carlo simulation. *J. Phys.: Cond. Mater.* **2006**, *18*, 3469–3478.

(119) Zha, C.-S.; Mao, H.-k.; Hemley, R. J. Elasticity of dense helium. *Phys. Rev. B: Condens. Matter Mater. Phys.* **2004**, *70*, 174107.

(120) Cohen, M. J.; Murrell, J. N. An analytic function for the three-body potential of  $\text{He}^3$ . *Chem. Phys. Lett.* **1996**, *260*, 371–376.

(121) Syshchenko, O.; Day, J.; Beamish, J. Frequency Dependence and Dissipation in the Dynamics of Solid Helium. *Phys. Rev. Lett.* **2010**, *104*, 195301.

(122) Barnes, A. L.; Hinde, R. J. Three-body interactions and the elastic constants of hcp solid  $\text{He}^4$ . *J. Chem. Phys.* **2017**, *147*, 114504.

(123) Cheng, Z. G.; Beamish, J. Mass Flow through Solid  $\text{He}^3$  in the bcc Phase. *Phys. Rev. Lett.* **2018**, *121*, 225304.

(124) Cencek, W.; Jeziorska, M.; Akin-Ojo, O.; Szalewicz, K. Three-Body Contribution to the Helium Interaction Potential. *J. Phys. Chem. A* **2007**, *111*, 11311–11319.

(125) Parish, C. A.; Dykstra, C. E. Three-body analytical potential for interacting helium atoms. *J. Chem. Phys.* **1994**, *101*, 7618–7624.

(126) Wang, L.; Sadus, R. J. Relationships between three-body and two-body interactions in fluids and solids. *J. Chem. Phys.* **2006**, *125*, 144509.

(127) Chang, S.-Y.; Boninsegni, M. Ab initio potentials and the equation of state of condensed helium at high pressure. *J. Chem. Phys.* **2001**, *115*, 2629–2633.

(128) Kihara, T.; Koba, S. Crystal Structures and Intermolecular Forces of Rare Gases. *J. Phys. Soc. Jpn.* **1952**, *7*, 348–354.

(129) Niebel, K.; Venables, J. An explanation of the crystal structure of the rare gas solids. *Proc. R. Soc. London A: Math., Phys. Eng. Sci.* **1974**, *336*, 365–377.

(130) van de Waal, B. W. Can the Lennard-Jones solid be expected to be fcc? *Phys. Rev. Lett.* **1991**, *67*, 3263–3266.

(131) Ackland, G. J.; Jones, A. P. Applications of local crystal structure measures in experiment and simulation. *Phys. Rev. B: Condens. Matter Mater. Phys.* **2006**, *73*, 054104.

(132) Krainyukova, N. V.; Boltnev, R. E.; Bernard, E. P.; Khmelenko, V. V.; Lee, D. M.; Kiryukhin, V. Observation of the fcc-to-hcp Transition in Ensembles of Argon Nanoclusters. *Phys. Rev. Lett.* **2012**, *109*, 245505.

(133) Loubeyre, P. Three-body-exchange interaction in dense rare gases. *Phys. Rev. B: Condens. Matter Mater. Phys.* **1988**, *37*, 5432–5439.

(134) Conway, J. H.; Goodman-Strauss, C.; Sloane, N. Recent progress in sphere packing. *Current Developments in Mathematics* **1999**, *1999*, 37–76.

(135) Conway, J. H.; Sloane, N. J. A. What are all the best sphere packings in low dimensions? *Discrete & Computational Geometry* **1995**, *13*, 383–403.

(136) Baxter, R. J. Percus-Yevick Equation for Hard Spheres with Surface Adhesion. *J. Chem. Phys.* **1968**, *49*, 2770–2774.

(137) Trombach, L.; Hoy, R. S.; Wales, D. J.; Schwerdtfeger, P. From sticky-hard-sphere to Lennard-Jones-type clusters. *Phys. Rev. E: Stat. Phys., Plasmas, Fluids, Relat. Interdiscip. Top.* **2018**, *97*, 043309.

(138) Stillinger, F. H. Lattice sums and their phase diagram implications for the classical Lennard-Jones model. *J. Chem. Phys.* **2001**, *115*, 5208–5212.

(139) Peterson, O. G.; Batchelder, D. N.; Simmons, R. O. Measurements of X-Ray Lattice Constant, Thermal Expansivity, and Isothermal Compressibility of Argon Crystals. *Phys. Rev.* **1966**, *150*, 703–711.

(140) Erradonea, D.; Boehler, R.; Japel, S.; Mezouar, M.; Benedetti, L. R. Structural transformation of compressed solid Ar: An x-ray diffraction study to 114 GPa. *Phys. Rev. B: Condens. Matter Mater. Phys.* **2006**, *73*, 092106.

(141) Troitskaya, E.; Pilipenko, E.; Gorbenko, I. I. Absolute Instability of FCC Lattice of Rare-Gas Crystals under Pressure. *Phys. Solid State* **2019**, *61*, 30–38.

(142) Pechenik, E.; Kelson, I.; Makov, G. Many-body model of rare gases at high pressures. *Phys. Rev. B: Condens. Matter Mater. Phys.* **2008**, *78*, 134109.

(143) Sherman, W. F. Pressure-induced changes in mode Gruneisen parameters and general equations of state for solids. *J. Phys. C: Solid State Phys.* **1982**, *15*, 9–23.

(144) Tilford, C. R.; Swenson, C. A. Thermal Expansions of Solid Argon, Krypton, and Xenon above 1 K. *Phys. Rev. B* **1972**, *5*, 719–732.

(145) Fugate, R.; Swenson, C. Specific heats of solid natural neon at five molar volumes and of the separated neon isotopes at  $P = 0$ . *J. Low Temp. Phys.* **1973**, *10*, 317–343.

(146) Feldman, C.; Feldman, J. L.; Horton, G. K.; Klein, M. L. Anharmonic contribution to the Gruneisen parameters of solid argon, krypton and xenon. *Proc. Phys. Soc., London* **1967**, *90*, 1182–1185.

(147) Lurie, J. B. On the Gruneisen parameter in the noble gas solids. *J. Low Temp. Phys.* **1973**, *10*, 751–757.

(148) Holste, J. C. *Thermal expansion of solid neon from 1 to 15 K*; Digital Repository, Iowa State University: 1973; <http://lib.dr.iastate.edu/>.

(149) Mausbach, P.; Köster, A.; Rutkai, G.; Thol, M.; Vrabec, J. Comparative study of the Grüneisen parameter for 28 pure fluids. *J. Chem. Phys.* **2016**, *144*, 244505.

(150) Gupta, N.; Gupta, R. Lattice dynamics of heavy rare-gas solids. *Can. J. Phys.* **1969**, *47*, 617–625.

(151) Batchelder, D. N.; Losee, D. L.; Simmons, R. O. Isotope Effects in the Lattice Constant and Thermal Expansion of  $^{20}\text{Ne}$  and  $^{22}\text{Ne}$  Single Crystals. *Phys. Rev.* **1968**, *173*, 873–880.

(152) Losee, D. L.; Simmons, R. O. Thermal-Expansion Measurements and Thermodynamics of Solid Krypton. *Phys. Rev.* **1968**, *172*, 944–957.

(153) Sears, D. R.; Klug, H. P. Density and Expansivity of Solid Xenon. *J. Chem. Phys.* **1962**, *37*, 3002–3006.

(154) Karasevskii, A. I.; Holzapfel, W. B. Equations of state and thermodynamic properties of rare-gas solids under pressure calculated using a self-consistent statistical method. *Phys. Rev. B: Condens. Matter Mater. Phys.* **2003**, *67*, 224301.

(155) Holzapfel, W. Effects of intrinsic anharmonicity in the Mie-Grüneisen equation of state and higher order corrections. *High Pressure Res.* **2005**, *25*, 187–203.

(156) de Souza, M.; Menegasso, P.; Paupitz, R.; Seridonio, A.; Lagos, R. E. Grüneisen parameter for gases and superfluid helium. *Eur. J. Phys.* **2016**, *37*, 055105.

(157) Wüest, A.; Merkt, F. Determination of the interaction potential of the ground electronic state of  $\text{Ne}_2$  by high-resolution vacuum ultraviolet laser spectroscopy. *J. Chem. Phys.* **2003**, *118*, 8807–8812.

(158) Muto, Y. Force between nonpolar molecules. *Proc. Phys. Math. Soc. Japan* **1943**, *17*, 629.

(159) Terras, A. A. Bessel series expansions of the Epstein zeta function and the functional equation. *Trans. Am. Math. Soc.* **1973**, *183*, 477–486.

(160) Nomura, R.; Okuda, Y. Colloquium: Quantum crystallizations of  $^4\text{He}$  in superfluid far from equilibrium. *Rev. Mod. Phys.* **2020**, *92*, 041003.

(161) Wallace, D. C. Anharmonic Free Energy of Crystals at High Temperatures. *Phys. Rev.* **1963**, *131*, 2046–2056.

(162) Wallace, D. C. Anharmonic Free Energy of Crystals at Low Temperatures and at Absolute Zero. *Phys. Rev.* **1964**, *133*, A153–A162.

(163) Dewaele, A. Private communication, 2020.

## ■ NOTE ADDED AFTER ASAP PUBLICATION

This paper published ASAP on March 31, 2021 with an error in eq (15). The paper was revised and reposted on April 2, 2021.